J. Fluid Mech. (1997), *vol.* 334, *pp.* 251–291

Copyright © 1997 Cambridge University Press

Dynamic simulation of freely draining flexible polymers in steady linear flows

By PATRICK S. DOYLE,
ERIC S. G. SHAQFEH AND ALICE P. GAST

Department of Chemical Engineering, Stanford University, Stanford, CA 94305-5025, USA

(Received 8 December 1995 and in revised form 3 October 1996)

We present a study of the rheological and optical behaviour of Kramers bead–rod chains in dilute solution using stochastic computer simulations. We consider two model linear flows, steady shear and uniaxial extensional flow, in which we calculate the non-Newtonian Brownian and viscous stress contribution of the polymers, their birefringence and a stress-optic coefficient. We have developed a computer algorithm to differentiate the Brownian from the viscous stress contributions which also avoids the order $(\delta t)^{-1/2}$ noise associated with the Brownian forces. The strain or shear rate is made dimensionless with a molecular relaxation time determined by simulated relaxation of the birefringence and stress after a strong flow is applied. The characteristic *long* relaxation time obtained from the birefringence and stress are equivalent and shown to scale with N^2 where N is the number of beads in the chain.

For small shear or extension rates the viscous contribution to the effective viscosity is constant and scales as N. We obtain an analytic expression which explains the scaling and magnitude of this viscous contribution. In uniaxial extensional flow we find an increase in the extensional viscosity with the dimensionless flow strength up to a plateau value. Moreover, the Brownian stress also reaches a plateau and we develop an analytic expression which shows that the Brownian stress in an aligned bead–rod chain scales as N^3. Using scaling arguments we show that the Brownian stress dominates in steady uniaxial extensional flow until large Wi, $Wi \approx 0.06N^2$, where Wi is the chain Weissenberg number. In shear flow the viscosity decays as $Wi^{-1/2}$ and the first normal stress as $Wi^{-4/3}$ at moderate Wi. We demonstrate that these scalings can be understood through a quasi-steady balance of shear forces with Brownian forces. For small Wi (in shear and uniaxial extensional flow) and for long times (in stress relaxation) the stress-optic law is found to be valid. We show that the rheology of the bead–rod chain can be qualitatively described by an equivalent FENE dumbbell for small Wi.

1. Introduction

The configurations of deformed polymer molecules in dilute solutions subject to flow manifest themselves in measurable quantities such as rheological coefficients and optical anisotropy. Understanding the polymer physics of these dilute solutions in simple flows is crucial in order to develop molecular models and constitutive equations which can subsequently be implemented for more complex flows and geometries.

Some of the earliest theoretical developments in equilibrium polymer physics involved polymer models constructed from spherical beads connected by rigid rods,

https://doi.org/10.1017/S0022112096004302 Published online by Cambridge University Press

i.e. bead–rod chains (Flory 1989). Kuhn (1934) and Guth & Mark (1934) showed that the probability distribution function for the separation of the chain ends for 'phantom' bead–rod chains is a Gaussian. Using statistical thermodynamics it can be shown (Treloar 1975) that the force required to increase the chain end-to-end separation is proportional to the end-to-end separation, i.e. the entropic force behaves as a Hookean spring for small deformations. For larger deformations Kuhn & Grun (1942) showed that the entropic force is given by the inverse Langevin function. These entropic forces derived from the bead–rod model are the fundamental starting point for most bead–spring models, where the spring represents the entropic force. Bead–spring dumbbell models have been studied extensively and have been useful in developing constitutive equations for polymer solutions (Bird *et al.* 1987; Doi & Edwards 1986; Larson 1988).

Until recently, the rheology of the bead–rod model has received relatively little attention due to the complexities associated with the constraints. Hassager (1974) was the first to examine the bead–rod model in steady uniaxial extensional flow. Hassager developed asymptotic expansions in the Péclet number, Pe, for the polymer extensional viscosity at small and large Pe and performed numerical calculations for three-bead chains. He showed that the polymer extensional viscosity increases by a factor of N, where N is the number of beads in the chain, from a low-Pe plateau to a high-Pe plateau.

Hinch (1976*a*) developed a theory for a continuous flexible string to examine the dynamics of a non-Brownian flexible fibre in shear flow. Hinch found that the chain would quickly orient in the flow direction and snap straight due to the tensions arising from the shear flow. Hinch (1976*b*) later examined the effect of weak Brownian motion on the flexible string via a diffusion equation in Fourier space. He found that the shortening of the end-to-end chain separation in linear flows depended on the degree of discretization which must be truncated to avoid an 'ultra-violet catastrophe'. The divergence occurs because each discretization imparts additional degrees of freedom to the chain thus increasing the entropic force. The concept is similar to the Debye theory for the heat capacity of crystals (McQuarrie 1973) where the atomic nature of the crystal must be included to truncate the highest frequency attainable in a crystal. In the bead–rod polymer model the cut-off also occurs due to molecular rigidity and the cut-off length scale is dictated by the rod size or Kuhn step. Thus the bead–rod model is simply a discretized form of the flexible string model considered by Hinch where the number of rods corresponds to the degree of discretization as well as a measure of the chain rigidity.

Ryckaert, Ciccotti & Berendsen (1977) developed two methods to handle rigid constraints in a molecular dynamics simulation to ensure that the inter-bead separation is a constant to within a specified tolerance at the end of a time step. The first is a method later implemented by Liu (1989) and the second is the well-known SHAKE algorithm (Allen & Tildesley 1987).

The bead–rod model has been helpful in understanding polymer dynamics in transient strong flows and the molecular basis for viscous stress. Simulations by Acierno, Titomanlio & Marrucci (1974) and by Rallison & Hinch (1988) of non-Brownian bead–rod chains in transient uniaxial flow showed that large viscous stresses can be attributed to the unfolding of *back loops* which prevent the chain from moving affinely with the flow. Recognizing that the unfolding of the back loops in the previous three-dimensional simulations can be well characterized by a one-dimensional non-Brownian string, Larson (1990) developed a novel ' kink dynamics' algorithm. Due to the simplicity of his model, he was able to simulate large chains ($N = 400$) and

https://doi.org/10.1017/S0022112096004302 Published online by Cambridge University Press

showed that the viscous stress scales with R_{end}^3 where R_{end} is the chain end-to-end distance. Recently Hinch (1994*b*) performed Brownian dynamics simulations of bead–rod chains and kink dynamics simulations in strong extensional flow. He suggests that the stress is mainly viscous and scales with R_g^4/N where R_g is the radius of gyration of the chain.

The rheological properties of short ($N \leqslant 20$) bead–rod chains in steady flows were examined by Liu (1989). He applied the constraint algorithm of Ryckaert *et al.* (1977) to the Brownian dynamics of bead–rod chains and demonstrated that the resulting algorithm is consistent with the Fokker–Planck equation for a bead–rod chain in kinetic theory (Bird *et al.* 1987). He confirmed the asymptotic expansions of Hassager (1974) for uniaxial extensional flow and in simple shear flow he found a shear-thinning polymer viscosity and first normal stress coefficient. Xu, Kim & Pablo (1994) performed similar calculations for a bead–rod chain with excluded volume and anisotropic friction in steady flows. The excluded volume tends to expand the configuration of the chain giving rise to a larger polymer shear viscosity and first normal stress coefficient. Anisotropic friction gives rise to a small negative second normal stress coefficient.

Grassia & Hinch (1996) have recently examined the stress relaxation of an initially straight bead–rod chain via Brownian dynamics. They employ a simulation algorithm developed by Grassia, Hinch & Nitsche (1995) which accounts for variable diffusivity and also includes pseudo-potential forces to convert the statistics from a rigid link system to an infinitely stiff bead–spring system (Hinch 1994*a*). Grassia & Hinch also develop a modified stress calculation to correctly calculate the Brownian stresses. They find $O(N^3)$ Brownian stresses for a straight chain decaying exponentially at long times with an $O(1/N^2)$ rate.

The previous work, with the exception of Grassia & Hinch (1996), either neglected or underestimated the polymer Brownian stresses. Our work differs substantially from that of Grassia & Hinch (1996) in that we consider birefringence, the effect of flow and the partitioning of the polymer stress into viscous and Brownian components which is crucial in the development of a constitutive equation for the polymer stress. Xu *et al.* (1994) did examine bead–rod chains in steady shear and extensional flow, but they did not differentiate the Brownian from the viscous stress, nor did they determine the long-time chain relaxation scaling which is necessary to express results in terms of the chain Weissenberg number Wi. Moreover, they did not attempt to calculate the optical properties of the chains, or determine universal scalings for the rheological material functions. Additionally, since we calculate the polymer optical anisotropy and stress, we can test the validity of the stress-optic law for bead–rod chains. This is fundamentally important since in many experiments it is assumed *a priori* that the stress tensor is proportional to the index of refraction tensor (Ramanathan, Headley & Lai 1995).

In this paper we present simulations of the rheological and optical properties of a dilute suspension of bead–rod chains in two model linear flows: simple shear and uniaxial extensional flow. The dimensionless flow strengths are characterized by a simulated Weissenberg number, Wi. The Brownian and viscous contributions to the polymer stress are explicitly calculated. In addition, the anisotropic polymer index of refraction and the stress optic coefficient for the chain are also calculated.

First, in §2 the bead–rod polymer model is developed in terms of a discretized continuous string neglecting inter-bead hydrodynamic and excluded volume interactions. The various forces acting on the chain, namely constraint, hydrodynamic and Brownian, produce a stochastic differential equation containing stochastic Brownian

https://doi.org/10.1017/S0022112096004302 Published online by Cambridge University Press

forces which must be interpreted in the Stratonovich sense (Gardiner 1985) in order to derive the Fokker–Planck equation corresponding to this model (Öttinger 1994). The Stratonovich interpretation of the stochastic terms will also be important in our polymer stress calculations described in §5.

In §3 the Brownian dynamics numerical simulation technique is discussed. The stochastic simulation of polymer models with rigid links is more complex than bead–spring simulations due to the constraint on the link length. Ermak & McCammon (1978) showed that the gradient of the diffusivity tensor must be incorporated into a Brownian dynamics algorithm when the diffusivity of a bead in the model depends on the chain configuration. Another way to account for the variable diffusivity is to use a second-order-time step algorithm (Fixman 1978; Grassia *et al.* 1995). Liu (1989) implemented the iterative simulation technique of Ryckaert *et al.* (1977) for bead–rod chains to ensure a constant link length at the end of a time step. We show in §3 that this algorithm is consistent with a second-order-time step algorithm and has the added benefit of ensuring that the link length is constant at all times. In §4 we non-dimensionalize the problem with the appropriate scalings.

The polymer contribution to the stress in a suspension and two methods of calculating it are discussed in §5. The first, the Giesekus form of the stress tensor, involves calculating the time derivative of a tensor as a function of bead position. This is not possible in our stochastic simulation because the chain trajectories are not smooth in time due to the Brownian forces (Gardiner 1985). The Giesekus stress tensor is convenient for steady-state results since it is only a function of the bead positions and the velocity gradient tensor. The second formulation for the polymer stress is based on the Kramers–Kirkwood stress tensor (Bird *et al.* 1987). In its usual form the Kramers–Kirkwood stress tensor contains $O(\delta t^{-1/2})$ fluctuations due to the $O(\delta t^{-1/2})$ Brownian forces that are often larger than the stress itself. Using the Stratonovich interpretation of the Brownian force we develop a technique to filter out the $O(\delta t^{-1/2})$ fluctuations while capturing the correct $O(1)$ correlations in the stress tensor. This second form of the stress tensor can be used to calculate the transient and steady-state polymer stress.

In §6 we discuss the Brownian and viscous contributions to the polymer stress and how to explicitly calculate them in a stochastic simulation. We study the simplest bead–rod chain, a rigid dumbbell, where the stress tensor is a simple function of the dumbbell orientation and the flow deformation tensor (Bird *et al.* 1987) to illustrate the nature of the Brownian and viscous stress, and as a check on our stress calculation technique. Lastly, we derive an expression for the limiting value for the Brownian stress corresponding to a fully extended chain of N beads which is shown to scale with N^3.

The optical anisotropy of a flowing suspension due to the presence of aligned polymer chain segments and the applicability of a stress-optic law for a bead–rod chain is discussed in §7.

In §8 we present results for the simulated relaxation of chains from an initial stretched configuration to their equilibrium configuration. The polymer birefringence, stress and stress-optic coefficient are calculated as the chains relax. The long-time stress and birefringence decay are fitted to a single exponential to yield a characteristic relaxation time, λ_1, for the chain. The relaxation time is then used to rescale the bead Pe to a chain Wi.

The steady-state rheology and optical properties of bead–rod chains in simple shear flow are discussed in §9. The material properties of the chains are separated into three separate regions of Wi having distinct dynamics. For small Wi, the viscous

https://doi.org/10.1017/S0022112096004302 Published online by Cambridge University Press

contribution to the shear viscosity is linear in N and an analytic expression is calculated by considering a chain composed of independent dumbbells. For moderate Wi, the polymer viscosity and first normal stress coefficient show power-law behaviour and collapse onto universal curves when plotted versus Wi. A power law for the polymer viscosity is derived by balancing the shear forces tending to stretch the chain with the entropic Brownian forces causing the chain to collapse into a compact configuration. The thinning of the polymer viscosity and first normal stress coefficient at moderate Wi are almost entirely due to the Brownian contributions, while the viscous contributions are relatively constant until large Wi where they show a slight increase before thinning. The stress-optic coefficient is relatively constant for small Wi and the magnitude agrees with that calculated from the relaxing chains in §8. The stress-optic law begins to fail for moderate Wi ($Wi \geqslant 3$) due to Brownian stresses which are a function of the correlated orientation of many rods.

In §10 the steady-state rheology and optical properties of a bead–rod chain in uniaxial extensional flow are discussed. We expand upon the early kinetic theory developments of Hassager (1974) for three-bead chains or trumbells in steady potential flow and develop integral expressions for the total, viscous and Brownian extensional viscosity which are subsequently evaluated numerically. Our kinetic theory results show excellent agreement with our stochastic simulations. We show that the asymptotic expressions in Pe developed by Hassager (1974) for the polymer extensional viscosity at small and large Pe show universal scaling behaviour when expressed in terms of Wi. Thus we predict a narrow but finite region of Wi where the polymer viscosity increases to its maximum value. We find that the initial increase in the viscosity with increasing Wi is mostly Brownian for large chains. This is explained by using the asymptotic expressions of Hassager and the $O(N^3)$ Brownian stresses predicted for a straight chain derived in §6. Lastly, the stress-optic coefficient is constant for small Wi and has the same magnitude as in the shear simulations in §9 and the relaxation simulations of §8.

Finally, in §11 we compare the bead–rod chain to the FENE dumbbell model. First we review the derivation of the FENE force law starting from a bead–rod chain. The average force required to hold the two ends of a bead–rod chain at a given separation is compared to the FENE force law and the inverse Langevin function. We find that a 10-bead chain is sufficient to recover the universal force-extension curve. Thereafter, we compare our simulations of FENE dumbbells in steady shear and uniaxial extensional flow to a bead–rod chain with 100 beads.

2. The polymer model

In our study, the polymer is modelled as a bead–rod chain, where the beads act as sources of friction and the rods serve as constraints to hold successive beads at a constant relative distance. The thermodynamics of a bead–rod chain with rigid-rod connectors is different than of a chain containing very stiff rods (Hinch 1994*a*). We have chosen to simulate rigid connectors so that we may utilize a rigorous simulation technique developed by Liu (1989) and so that we may compare to the kinetic theory results of Hassager (1974). Furthermore, the rheology of a bead–rod chain with rigid connectors is not significantly different than that of a chain with stiff connectors: the Brownian stress when the chain is fully aligned does not differ, the zero shear viscosity does not differ (Bird *et al.* 1987), and we have performed simulations to show that the viscous contribution to the zero shear viscosity only differs by less than 1%.

A bead–rod chain is completely analogous to a discretized flexible inextensible

https://doi.org/10.1017/S0022112096004302 Published online by Cambridge University Press

string in which the size of the discretization corresponds to the rod size in the bead–rod model. We shall refer to the flexible inextensible string model to guide the development of our governing equations. The connecting rods physically correspond to Kuhn steps and thus they act as the smallest rigid length scale in the model. By increasing the number of beads in a chain of constant length we will decrease the Kuhn length relative to the chain length – in effect making the chain more flexible. With this model, the chain dynamics can be described by a stochastic diffusion equation (Liu 1989; Öttinger 1994; Grassia & Hinch 1995), and one can compute sample trajectories of the chain. These trajectories represent a sampling of the configuration space of the chain. To derive the governing equations we consider the form of all the forces in the system: hydrodynamic, constraint, and Brownian.

The hydrodynamic force on a bead is assumed to be linear in the slip velocity between the bead and the solvent velocity at the bead centre, if the inertia of the fluid is neglected. Thus,

$$F_i^{h,v} = -\xi_{ij}(\dot{r}_j^v - u_j^\infty(r_j^v)), \tag{2.1}$$

where ξ_{ij} is a general drag or resistance tensor, $\dot{r}_j^v$ is the velocity of bead v and $u_j^\infty(r_j^v)$ is the undisturbed solvent velocity. In our studies we limited ourselves to linear flows where the shear rate, $\dot{\gamma}$, or extension rate, $\dot{\epsilon}$, rate is defined by

$$\frac{\partial\, u_i^\infty}{\partial x_j} = \begin{cases} \kappa_{ij}\dot{\gamma} & \text{shear flow} \\ \kappa_{ij}\dot{\epsilon} & \text{extensional flow,} \end{cases} \tag{2.2}$$

and κ_{ij} is defined by:

$$\kappa_{ij} = \begin{cases} \delta_{i1}\delta_{j2} & \text{shear flow} \\ \delta_{i1}\delta_{j1} - 0.5\delta_{i2}\delta_{j2} - 0.5\delta_{i3}\delta_{j3} & \text{extensional flow.} \end{cases} \tag{2.3}$$

Note that we have neglected any hydrodynamic interactions between the beads. In addition, all simulations discussed in this paper were performed with an isotropic drag tensor

$$\xi_{ij} = \delta_{ij}\, 6\pi\, \mu\, b = \delta_{ij}\, \xi \tag{2.4}$$

where b is the bead radius. We have also completed simulations employing an anisotropic drag tensor to account for the anisotropic drag that occurs on a slender continuous body. These simulations were more computationally expensive and were not qualitatively different.

The constraint forces were derived by considering the chain to be a discretized flexible inextensible string. The constraint force per unit length in a string is equal to the gradient in the tension (Hinch 1976*a*):

$$f_i^c(s) = \frac{\partial[T(s)\rho_i(s)]}{\partial s}, \tag{2.5}$$

where $\rho_i(s)$ is a unit vector tangent to the string and s is the arclength variable. By integrating (2.5) over the length of a single rod, it follows that the discrete constraint force acting on bead v takes the form

$$F_i^{c,v} = T^v u_i^v - T^{v-1} u_i^{v-1}, \tag{2.6}$$

where T^v is the tension in the vth rod of length a and orientation $u_i^v = (r_i^{v+1} - r_i^v)/a$. The rods are thus a discrete means of representing the internal forces associated with a flexible inextensible body. The same constraint forces can be derived using the method of undetermined Lagrange multipliers (Allen & Tildesley 1987).

During a time step the polymer experiences numerous collisions with the solvent

https://doi.org/10.1017/S0022112096004302 Published online by Cambridge University Press

molecules. Neglecting the effects due to the constraints (to which we shall return in due course), these Brownian forces are approximated as a δ-correlated, white-noise process (Gardiner 1985) such that

$$\langle F_i^{br,v}(t)\rangle = 0, \tag{2.7}$$

$$\langle F_i^{br,v}(t)F_j^{br,\mu}(t')\rangle = 2kT\xi\ \delta_{v\mu}\ \delta_{ij}\ \delta(t-t'), \tag{2.8}$$

where $\delta_{v\mu}$ and δ_{ij} are Kronecker delta tensors and $\delta(t-t')$ is the Dirac delta function. The $2kT\xi$-term results from satisfying the fluctuation dissipation theorem in the absence of constraints (Russel, Saville & Schowalter 1989).

A discrete form for the Brownian forces during an individual time step beginning at time t and ending at time $t+\delta t$ is therefore

$$\langle F_i^{br,v}(\tau)\rangle = 0, \tag{2.9}$$

$$\langle F_i^{br,v}(\tau)F_j^{br,\mu}(\tau)\rangle = \frac{2kT\xi\ \delta_{v\mu}\ \delta_{ij}}{\delta t}, \tag{2.10}$$

where τ is equal to $t+\varsigma\ \delta t$. We note that when the Brownian forces are included in this manner, they have a magnitude proportional to $(\delta t)^{-1/2}$ and the sample trajectories will be continuous but the time derivative of the paths (or the *velocity*) will be discontinuous. The value of the dimensionless parameter ς depends on the interpretation of the stochastic process and can take values from 0 to 1 (Gardiner 1985; Öttinger 1995). Setting ς equal to $1/2$ corresponds to a Stratonovich interpretation (Gardiner 1985; Liu 1989) of the stochastic term. This interpretation is necessary to derive the correct corresponding Fokker–Planck equation from the stochastic equation (Liu 1989; Öttinger 1994). This is equivalent to stating that the Brownian forcing occurs throughout the time step and thus the beginning and end must be equally weighted.

3. Numerical simulation

Care must be taken to construct a valid simulation algorithm when rigid constraints are employed. A simple first-order time-stepping algorithm is inadequate due to the variable effective diffusivity of the beads (Ermak & McCammon 1978). Additionally, the inter-bead distance is not held constant with a non-iterative scheme. Liu (1989) proposed an iterative simulation technique to constrain the inter-bead distance within a specified tolerance. Liu demonstrated the equivalence of his numerical algorithm to a corresponding Fokker–Planck equation. In our studies we have used Liu's numerical algorithm to produce sample chain trajectories. We shall show that Liu's algorithm is equivalent to a mid-point scheme, and thus correctly accounts for variable diffusivity (Grassia *et al.* 1995).

Neglecting chain inertia, the forces on the beads sum to zero,

$$F_i^{br,v} + F_i^{c,v} + F_i^{h,v} = 0. \tag{3.1}$$

Expressing the hydrodynamic force in terms of the bead and solvent velocity, equation (3.1) can be rewritten as

$$\dot{r}_i^v(t+\delta t/2) = \frac{1}{\xi}\left[F_i^{v,br}(t+\delta t/2) + F_i^{v,c}(t)\right] + u_i^{\infty}(r_i^v(t)). \tag{3.2}$$

In (3.2) the bead velocity is evaluated at time $t+\delta t/2$ due to the Stratonovich nature of the Brownian force. Evaluating the hydrodynamic forces at time t results in an

https://doi.org/10.1017/S0022112096004302 Published online by Cambridge University Press

order $(\delta t)^{1/2}$ error and simplifies the calculations. The directions of the constraint forces are evaluated at time t but their magnitude is determined by satisfying the constraints at $t+\delta t/2$. The beads are subject to the constraint

$$u_i^v\left(t+\delta t/2\right)u_i^v\left(t+\delta t/2\right)-1=0, \tag{3.3}$$

and the time derivative of (3.3) becomes

$$\dot{u}_i^v\left(t+\delta t/2\right)u_i^v\left(t+\delta t/2\right)=0. \tag{3.4}$$

Thus a link must have a velocity perpendicular to its orientation in order to maintain a constant length. The link orientation at time $t+\delta t/2$ can be approximated by a mid-point algorithm. Liu's iterative algorithm, based on the constraint

$$u_i^v(t+\delta t)u_i^v(t+\delta t)-1=0, \tag{3.5}$$

correctly satisfies the constraints while also rigorously maintaining a constant bead separation. This can be rewritten as

$$\left[\dot{u}_i^v(t+\delta t/2)\,\delta t+u_i^v(t)\right]\quad\left[\dot{u}_i^v(t+\delta t/2)\,\delta t+u_i^v(t)\right]-1=0, \tag{3.6}$$

$$\dot{u}_i^v(t+\delta t/2)\delta t\,\left[\dot{u}_i^v(t+\delta t/2)\delta t+u_i^v(t)\right]+u_i^v(t)\,\dot{u}_i^v(t+\delta t/2)\,\delta t+u_i^v(t)\,u_i^v(t)-1=0, \tag{3.7}$$

$$\dot{u}_i^v(t+\delta t/2)\,\left[u_i^v(t+\delta t)+u_i^v(t)\right]=0. \tag{3.8}$$

Approximating $u_i^v(t+\delta t/2)$ as $[u_i^v(t+\delta t)+u_i^v(t)]/2$ gives

$$\dot{u}_i^v\left(t+\delta t/2\right)u_i^v\left(t+\delta t/2\right)=0. \tag{3.9}$$

Thus constraining the rod size to be a constant at the end of a time step ensures that the velocity of a link at $t+\delta t/2$ is perpendicular to its orientation, which is consistent with a mid-point algorithm.

We conclude this section with a brief overview of the integration scheme used in our simulations, while a more thorough description can be found in Liu (1989). At the beginning of each time step an unconstrained move, denoted by t^*, is made:

$$r_i^v(t^*)=r_i^v(t)+\left[u_i^\infty(r_i^v(t))+\frac{F_i^{br,v}}{\xi}\right]\delta t. \tag{3.10}$$

The bead positions are subject to the constraint

$$[r_i^{v+1}(t+\delta t)-r_i^v(t+\delta t)]\,[r_i^{v+1}(t+\delta t)-r_i^v(t+\delta t)]-a^2<\varphi, \tag{3.11}$$

where φ is small and $r_i^v(t+\delta t)$ is given by

$$r_i^v(t+\delta t)=r_i^v(t^*)+\left[\frac{T^v u_i^v-T^{v-1}u_i^{v-1}}{\xi}\right]\delta t. \tag{3.12}$$

Combining equations (3.10), (3.11) and (3.12) leads to $N-1$ nonlinear equations for the tensions. The nonlinear term is small relative to the linear terms and thus the $N-1$ linear equations can be solved iteratively (Liu 1989). Two iterations of the equations are equivalent, to leading order in δt, to a mid-point algorithm.

To begin the simulation a random-walk polymer configuration is generated by choosing successive bead positions from random vectors distributed over the surface of a sphere. We realize that the equilibrium configuration of a rigid bead–rod system is not a random walk (Kramers 1946; Hassager 1974; Hinch 1994*a*), but it is a quick initial approximation and we can allow the chain to equilibrate for 10^5 to 5×10^6

https://doi.org/10.1017/S0022112096004302 Published online by Cambridge University Press

steps during which the solvent velocity, u_i^∞ is set to zero. After the equilibration period the chains are in their thermodynamic equilibrium state. Thereafter, u_i^∞ is introduced at its desired value. We assume ergodicity to obtain steady-state averages from time averages of a single chain taken over 10^7 to 10^8 time steps. For transient, or time-dependent results, actual ensemble averages are taken of 500 to 4000 chains. The size of the time step per simulation depends on the Péclet number and flow type.

4. Dimensions

We non-dimensionlize the problem by scaling lengths with the inter-bead separation a, forces with the thermal scale kT/a and time with $\xi a^2/kT$. The dimensionless parameter that arises from this scaling is a bead Péclet number. The Péclet number, $Pe = \dot{\gamma}\xi a^2/kT$ (or $\dot{\epsilon}\xi a^2/kT$), is the ratio of the time for a bead to freely diffuse a distance a to the flow time scale $1/\dot{\gamma}$ (or $1/\dot{\epsilon}$). A bead–rod chain has a spectrum of relaxation times, with $\xi a^2/kT$ being on the order of the fastest relaxation time. The slowest relaxation time, defined as $\lambda_1(N)\ \xi a^2/kT$, can be used to define a Weissenberg number, $Wi = \lambda_1(N)\dot{\gamma}\xi a^2/kT$, which is a measure of the chain relaxation made dimensionless with the flow time scale. We will calculate $\lambda_1(N)$ in our simulations discussed in §8 and thereafter we will present our results using both Pe and Wi.

5. Stress tensor

Calculating the stress contribution from the polymer model is a non-trivial matter because of the rigid constraints. In this section we will discuss the calculation of the stress tensor at steady state as well as under transient conditions.

The total stress in a flowing suspension of model polymers is the sum of the polymer and solvent contributions,

$$\sigma_{ij} = \sigma_{ij}^p + \sigma_{ij}^s \tag{5.1}$$

and can be expressed as (Bird *et al.* 1987)

$$\begin{aligned}\sigma_{ij} &= \tau_{ij} - P\delta_{ij} \\ &= \tau_{ij}^p - P^p\delta_{ij} + \tau_{ij}^s - P^s\delta_{ij},\end{aligned} \tag{5.2}$$

where $\tau_{ij} = \tau_{ij}^p + \tau_{ij}^s$ and $P = P^p + P^s$. τ_{ij} is defined to be zero at equilibrium and P is an isotropic pressure contribution.

The polymer contribution to τ_{ij} is given by the Kramers–Kirkwood stress tensor as the moment of the hydrodynamic forces

$$\tau_{ij}^p = \sum_{v=1}^{N} \langle R_i^v F_j^{h,v} \rangle \tag{5.3}$$

where R_i^v is the bead position relative to the chain centre of mass and $\langle \cdots \rangle$ denotes an ensemble average. Note that τ_{ij}^p has been made dimensionless with $n_p kT$ where n_p is the number density of polymer chains. Due to the force balance on the beads, the stress can also be expressed as

$$\tau_{ij}^p = -\sum_{v=1}^{N} \langle R_i^v F_j^{br,v} + R_i^v F_j^{c,v} \rangle. \tag{5.4}$$

https://doi.org/10.1017/S0022112096004302 Published online by Cambridge University Press

In this form, τ_{ij}^{p} is numerically difficult to evaluate because the Brownian and constraint forces have stochastic noise of the order $(\delta t)^{-1/2}$. We have developed a modified form of the Kramers–Kirkwood stress tensor that filters out the noise contributions of order $(\delta t)^{-1/2}$. The filtering technique is consistent with the Stratonovich interpretation of the stochastic forces and makes use of the correlations defined in equations (2.9) and (2.10). Starting with equation (5.4), we will consider each term separately. The first term we will write as

$$-\left\langle \tfrac{1}{2}\left[R_i^{\nu}(t)+R_i^{\nu}(t+\delta t)\right] F_j^{br,\nu}(t+\delta t/2)\right\rangle \tag{5.5}$$

due to the Stratonovich nature of the Brownian force. Recognizing that the Brownian force is uncorrelated with the bead position at the beginning of a time step we can rewrite equation (5.5) as

$$-\left\langle \tfrac{1}{2}\left[R_i^{\nu}(t+\delta t)\right] F_j^{br,\nu}(t+\delta t/2)\right\rangle . \tag{5.6}$$

We can expand $R_i^{\nu}(t+\delta t)$ in a Taylor series about the initial position at time t as $R_i^{\nu}(t)+O(\delta t)^{1/2}$ and subtract from it $R_i^{\nu}(t)$ which is again uncorrelated to the Brownian forces at time $(t+\delta t/2)$. This leads to

$$-\left\langle \tfrac{1}{2}\left[R_i^{\nu}(t+\delta t)-R_i^{\nu}(t)\right] F_j^{br,\nu}(t+\delta t/2)\right\rangle . \tag{5.7}$$

By making this transformation we are taking the time average of a displacement of order $(\delta t)^{1/2}$ multiplied by a stochastic force of order $(\delta t)^{-1/2}$ which is an $O(1)$ quantity. Thus we have avoided noise of order $(\delta t)^{-1/2}$ while still capturing the correct correlations.

Order $(\delta t)^{-1/2}$ noise still exists in the stress calculation due to the constraint forces. This noise originates in the first iteration of the matrix equations necessary to solve for the tensions. There are also $O(1)$ contributions after the first iteration which we need to preserve. We can distinguish the order $(\delta t)^{-1/2}$ terms by solving an auxiliary set of equations containing only Brownian forces while neglecting the solvent velocity. The forces (Brownian and tension) on the beads are again summed and set to zero, but now are solved subject to the constraint that the link velocity is perpendicular to the link direction at the beginning of a time step. Let $T^{*,\nu}$ and $F_i^{*,\nu}$ denote these tensions and constraint forces respectively. This leads to the following $N-1$ linear equations for $T^{*,\nu}$:

$$[F_i^{br,\nu+1}(t+\delta t/2)-F_i^{br,\nu}(t+\delta t/2)]u_i^{\nu}(t)+T^{*,\nu+1}u_i^{\nu+1}(t)u_i^{\nu}(t)-2T^{*,\nu} +T^{*,\nu-1}u_i^{\nu-1}(t)u_i^{\nu}(t)=0. \tag{5.8}$$

We note that due to the explicit constraint, only one iteration of a tridiagonal matrix is needed at each time step to solve for the tensions. These forces are the components of the total tension force which are order $(\delta t)^{-1/2}$ and are only correlated to $R_i^{\nu}(t+\delta t)$. A valid form for the stress contribution from the constraints is then

$$-\left\langle \left[\frac{R_i^{\nu}(t+\delta t)+R_i^{\nu}(t)}{2}\right]\left[F_j^{c,\nu}(t)-F_j^{*,\nu}(t)\right]+\left[\frac{R_i^{\nu}(t+\delta t)-R_i^{\nu}(t)}{2}\right]F_j^{*,\nu}(t)\right\rangle . \tag{5.9}$$

Combining these terms then we can avoid the $(\delta t)^{-1/2}$ noise in the stress evaluation. An equivalent algorithm to avoid the stochastic noise in the stress calculation has recently been introduced from a different approach by Grassia & Hinch (1996).

The above algorithm is necessary to evaluate the stress tensor in transient or time-dependent simulations, but the simpler Giesekus form can also be used to obtain

https://doi.org/10.1017/S0022112096004302 Published online by Cambridge University Press

steady-state stresses in stochastic simulations. The Giesekus form of the stress tensor is

$$\tau_{ij}^{p} = -\frac{1}{2}\frac{\mathsf{d}}{\mathsf{dt}}\sum_{v=1}^{N}\langle R_i^v R_j^v\rangle \tag{5.10}$$

where d/dt denotes a co-deformational derivative

$$\frac{\mathsf{d}}{\mathsf{dt}}Q_{ij} = \frac{\mathrm{d}Q_{ij}}{\mathrm{d}t} - Pe(\kappa_{ik}Q_{kj} + Q_{ik}\kappa_{kj}^{\dagger}), \tag{5.11}$$

which is equivalent to the Kramers–Kirkwood stress tensor (Bird *et al.* 1987).

Note that the Giesekus stress tensor involves calculating the time derivative of a sample trajectory. The time derivatives cannot be calculated explicitly because our stochastic simulation produces sample paths which are not time differentiable; however, for steady-state stress calculations, the time derivative may be set to zero and the Giesekus stress tensor becomes simply

$$\tau_{ij}^{p,ss} = \frac{1}{2}\sum_{v=1}^{N}\langle Pe\kappa_{ik}R_k^v R_j^v + Pe\kappa_{kj}^{\dagger}R_i^v R_k^v\rangle, \tag{5.12}$$

an expression in terms of the bead positions alone. This is not only computationally more efficient than the alternative stress algorithm, but also provides insight into those polymer configurations making the largest contribution to any particular element of the steady-state stress tensor.

6. Brownian versus viscous stress

Distinguishing the Brownian from the viscous stresses is crucial if one wants to determine the validity of various constitutive models in capturing the complex rheological behaviour of a polymer or a polymer model. In this section we discuss the origin of the two stress contributions, as well as how to calculate them in a stochastic simulation. Finally we derive an analytic expression for the maximum Brownian stress contribution from a polymer fully aligned by an arbitrarily strong flow field.

Viscous stress is due to the polymer's inability to move affinely with the deterministic flow field in the absence of Brownian forces. Brownian stresses are associated with the tendency of Brownian forces to randomize the polymer configuration. Both stresses depend upon the polymer configuration and this configuration is in turn determined by both the Brownian and flow forces. The easiest way to distinguish these contributions in an experiment is to simply turn off the flow field. The instantaneous or 'short time' stress remaining is due solely to the Brownian forces.

This distinction can be made clearer if we examine the stress contribution from a rigid dumbbell. For rigid dumbbells the polymer stress can be written as (Larson 1988)

$$\tau_{ij}^{dumbbell} = \left[-\delta_{ij} + 3\langle u_i u_j\rangle + \tfrac{1}{2}Pe\kappa_{kl}\langle u_i u_j u_k u_l\rangle\right], \tag{6.1}$$

where u_i is a unit vector defining the dumbbell orientation. The first two terms represent the Brownian stresses and the last is the viscous stress. While the Brownian stresses seem to be independent of $Pe\kappa_{ij}$, they are not really since u_i is determined by both the thermal and flow forces (Bird *et al.* 1987). Furthermore, it is apparent that setting $\kappa_{ij} = 0$ will effectively remove the viscous stresses.

In our simulations we can easily solve for the viscous stress by setting the Brownian

https://doi.org/10.1017/S0022112096004302 Published online by Cambridge University Press

	Equation (5.4)			Equation (6.1)			Stewart & Sorensen (1972)
Pe	$\eta^{viscous}$	$\eta^{Brownian}$	η^{total}	$\eta^{viscous}$	$\eta^{Brownian}$	η^{total}	η^{total}
1	0.0331	0.0489	0.0820	0.0334	0.0477	0.0811	0.0830
10	0.0366	0.0310	0.0676	0.0367	0.0308	0.0673	0.0675
100	0.0274	0.00276	0.0304	0.0274	0.00274	0.0301	0.0299

TABLE 1. Rigid dumbbell shear viscosity

forces to zero at the beginning of a time step and solving for the tensions. Only one iteration of the matrix equations is needed since the Brownian forces are neglected. The viscous stress is then

$$\tau_{ij}^{p,visc} = -\sum_{v=1}^{N} \langle R_i^v(t) F_j^{cvisc,v}(t) \rangle \tag{6.2}$$

where $F_j^{cvisc,v}$ is the constraint force obtained when the Brownian forces are neglected. The Brownian stresses could be also be determined separately, but since we already have calculated the total and viscous polymer stress, we need only subtract the viscous from the total to obtain the Brownian contribution. We note that the Brownian polymer stress has contributions from both the Brownian and constraint forces.

To verify that we are in fact correctly calculating the total stress as well as correctly distinguishing the Brownian from the viscous stresses, we have performed several simulations of dumbbells in shear flow. The steady-state shear viscosity and first normal stress calculated from our algorithm and equation (6.1) are shown along with the results of Stewart & Sorensen (1972) in table 1. We see excellent quantitative agreement confirming the validity of our stress algorithm.

Lastly, we expect to see a plateau in the Brownian stress in flows strong enough to fully unravel the polymer coil and align the connecting rods. For convenience we briefly switch from indicial to Gibbs notation. From the kinetic theory of bead–rod chains, the polymer stress (Liu 1989) for the chain can be written as

$$\begin{aligned} \boldsymbol{\tau}^p = & \sum_{i,j=1}^{N-1} \langle Pe \hat{C}^{ij} \boldsymbol{\kappa} : \boldsymbol{u}^j \boldsymbol{u}^j \boldsymbol{u}^i \boldsymbol{u}^i \rangle + 6 \sum_{i,j=1}^{N-1} \langle \hat{C}^{ij} \boldsymbol{u}^i \boldsymbol{u}^j \rangle \\ & + \left[\sum_{i,j=1}^{N-1} A^{ij} \langle \hat{C}^{ij} \boldsymbol{u}^j \boldsymbol{u}^j \rangle - \sum_{i,j,k,l=1}^{N-1} A^{ik} A^{il} \langle \hat{C}^{ij} \hat{C}^{kl} (\boldsymbol{u}^k \cdot \boldsymbol{u}^l) \boldsymbol{u}^i \boldsymbol{u}^j \rangle \right] \\ & - (N-1)\boldsymbol{\delta}. \end{aligned} \tag{6.3}$$

where

$$A^{ij} = \begin{cases} 2 & \text{if } i = j \\ -1 & \text{if } i = j \pm 1 \\ 0 & \text{otherwise.} \end{cases} \tag{6.4}$$

$\hat{C}^{ij}$ is defined by the relation

$$\sum_{j=1}^{N-1} (\boldsymbol{u}^i \cdot \boldsymbol{u}^j) A^{ij} \hat{C}^{jk} = \delta^{ik} \tag{6.5}$$

and $\boldsymbol{u}^i = \boldsymbol{R}^{i+1} - \boldsymbol{R}^i$.

https://doi.org/10.1017/S0022112096004302 Published online by Cambridge University Press

Let the polymer orientation be n_i such that $u_i^v = n_i$. The last four terms in equation (6.3) are the Brownian stress and can be simplified to

$$\tau_{ij}^p = \left[\tfrac{1}{3}N^3 + \tfrac{2}{3}N - 1\right] n_i n_j - (N-1)\delta_{ij}. \tag{6.6}$$

Using a different approach, Grassia & Hinch (1996) have independently derived equation (6.6) and showed that the tensions in the connecting rods are of the correct magnitude to satisfy the inextensibility constraint. Thus the leading-order term in the Brownian stress from a straight bead–rod chain scales as N^3. For comparison, the Brownian stress in a rigid bead–rod chain is independent of N. The difference lies in the fact that in a bead–rod chain each added bead gives the chain two additional degrees of freedom, while a rigid bead–rod chain has its degrees of freedom fixed at five. In addition, the viscous stress from a bead–rod chain aligned along the primary axis of extension scales with N^3Pe. Thus if the chain can be unravelled at Pe less than 1, the Brownian stress will be larger than the viscous.

7. Birefringence and stress-optic law

The birefringence is a measure of the optical anisotropy of a medium. For polymer solutions, birefringence is a sensitive measure of the average conformation of the polymer molecules. In our simulations each connecting rod in the chain is assigned a polarizability α_1 parallel to the rod and α_2 perpendicular to it. The anisotropic polymer contribution to the polarizability tensor α_{ij}^p is the sum of the individual rod polarizability tensors (Larson 1988)

$$\alpha_{ij}^p = n_p(\alpha_1 - \alpha_2) \sum_{v=1}^{N-1} u_i^v u_j^v. \tag{7.1}$$

The index-of-refraction tensor is proportional to the polarizability tensor through the Lorentz–Lorenz formula:

$$n_{ij}^p = A\alpha_{ij}^p, \tag{7.2}$$

where A is a function of the isotropic part of the index of refraction. We non-dimensionalize the index of refraction with $n_pA(\alpha_1 - \alpha_2)$, and thus the computed dimensionless polymer index of refraction is a measure of the average orientation of the connecting rods in the chain.

The birefringence, Δ', is the difference in the principle eigenvalues of the index-of-refraction tensor. For light propagating along the '3'-direction the birefringence is (Fuller 1990)

$$\Delta' = \left[\left(\sum_{v=1}^{N-1}\langle u_1^v u_1^v - u_2^v u_2^v\rangle\right)^2 + 4\left(\sum_{v=1}^{N-1}\langle u_1^v u_2^v\rangle\right)^2\right]^{1/2} \tag{7.3}$$

where Δ' has been made dimensionless with $n_pA(\alpha_1 - \alpha_2)$. The extinction angle, χ, measures the orientation of the principal axis from the '1'-direction

$$\tan(2\chi) = \frac{2\sum_{v=1}^{N-1}\langle u_1^v u_2^v\rangle}{\sum_{v=1}^{N-1}\langle u_1^v u_1^v - u_2^v u_2^v\rangle}. \tag{7.4}$$

For shear and uniaxial extensional flow the dimensionless birefringence will be zero

https://doi.org/10.1017/S0022112096004302 Published online by Cambridge University Press

at equilibrium and have a maximum possible value of $N-1$. The extinction angle in shear flow for small Wi is initially 45° and can decrease to a minimum of 0°. Due to the symmetry of extensional flow, the extinction angle is a constant for all Wi and is not of interest.

In addition to measuring the average chain conformation, birefringence can potentially measure the polymer stress if the stress-optic law is valid for the system (Wales 1976; Larson 1988; Kannan & Kornfield 1994). The stress-optic law states that the polymer stress is proportional to the index-of-refraction tensor. A stress-optic coefficient for the chain is usually defined by the relation

$$n_{ij}^{p} = C\ \sigma_{ij}^{p}. \tag{7.5}$$

We note that the most general form for the stress-optic relation is through a fourth-order tensor $C_{ijkl}(Wi)$. In the present study we have limited ourselves to testing the validity of equation (7.5) since it is the most commonly assumed form for the stress-optic law. Kuhn & Grun (1942) have shown for small deformations of a bead–rod chain that $\sum_{v=1}^{N-1} \langle u_i^v u_j^v \rangle \propto \langle R_i^{end} R_j^{end} \rangle$ where R_i^{end} is a vector directed from one end of the chain to the other. If the stress due to the bead–rod chain is approximated using a Hookean dumbbell (Treloar 1975), then the stress will also be proportional to $\langle R_i^{end} R_j^{end} \rangle$ and the stress-optic law will hold. Note that the major assumptions are small deformations from the equilibrium configuration and a purely entropic or Brownian stress proportional to $\langle R_i^{end} R_j^{end} \rangle$.

In our simulations the polymer stress is a complicated function of u_i^v and has both Brownian and viscous contributions. The viscous stress scales with Wi and thus must be small relative to the Brownian contribution for C to be constant. Furthermore, if the rod orientations are uncorrelated, as found near equilibrium, then the tensor $\hat{C}_{ij}$ in equation (6.5) is to a first approximation isotropic. Using this approximation in equation (6.3) leads to a Brownian stress proportional to $\sum_{v=1}^{N-1} \langle u_i^v u_j^v \rangle$. Thus we expect the bead–rod chain to have an approximately constant stress-optic coefficient if the stress is mostly Brownian and the chain is only slightly distorted from its equilibrium configuration. We check the stress-optical rule in our simulations over a wide range of flow strengths as described below.

8. Chain time scales

The relaxation of an uncoiled polymer chain occurs over many times scales and can be characterized by a spectrum of relaxation times. The slowest relaxation process yields a dimensionless characteristic relaxation constant λ_1 for the chain. This time may be used to rescale our Péclet number and thus define a Weissenberg number, Wi:

$$Wi = \lambda_1\ Pe. \tag{8.1}$$

The Weissenberg number is thus the product of the chain relaxation time and the shear rate and is more indicative of the flow strength than the Péclet number for a polymer chain. Furthermore, in an experiment, one can measure the chain relaxation after applying a strong flow and use this value to present the results in terms of an experimental Wi to be compared directly with simulations. We have performed simulations of chains which are initially uncoiled and aligned in the '1'-direction. This initial configuration corresponds to a chain placed in uniaxial extensional flow as

https://doi.org/10.1017/S0022112096004302 Published online by Cambridge University Press

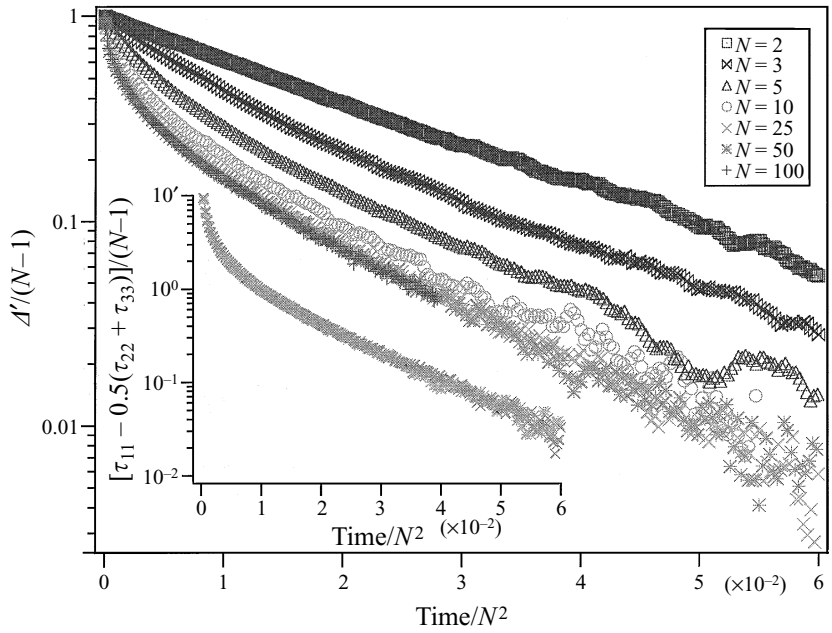


FIGURE 1. Birefringence scaled by $(N-1)$ versus t/N^2 for an initially straight chain aligned in the '1'-direction for $N = 2, 3, 5, 10, 25, 50, 100$. The inset graph shows the polymer stress, $[\tau_{11} - 0.5(\tau_{22} + \tau_{33})]/(N-1)$, versus t/N^2 for $N = 25, 50, 100$.

$Wi \to \infty$. As an ensemble of 500–4000 chains relax, we calculate the average transient stress and the birefringence.

We anticipate that at long times the relaxation of the birefringence will decay exponentially and λ_1 will scale with the square of the number of connecting rods, N^2, for long chains (Larson 1988). This is analogous to the slowest mode of a Rouse chain (Doi & Edwards 1988). As the chain relaxes, correlations in the directions of the connecting rods vanish and the stress is proportional to $(N-1)\langle u_i u_j \rangle$ where u_i is the average orientation of the rods. Thus at long times the stress will be proportional to the birefringence and a relatively constant stress-optic coefficient is expected. In figure 1 we show the birefringence normalized with $N-1$ versus t/N^2 and, in the inset, we show the stress normalized with $N-1$ versus t/N^2. We have fit the linear region of the semi-log plots with a single exponential of the form Ae^{-t/λ_1} and show the results for λ_1 in table 2. The λ_1 values obtained from fitting the decay of stress and birefringence are identical to within the statistical error of the simulations. Our stress relaxation times are consistent with the recent work of Grassia & Hinch (1996). The transient stress-optic coefficient is shown in figure 2. The value of C not only approaches a constant for long times, but converges to a value independent of N for large N. Thus for small perturbations to the equilibrium chain configuration the dimensionless Brownian stress is approximately

$$\lim_{N\to\infty} \tau_{ij}^{p} \approx 5 \sum_{\nu=1}^{N-1} \langle u_i^{\nu} u_j^{\nu} \rangle. \tag{8.2}$$

This is in agreement with the theoretical stress-optic coefficient derived by Kuhn & Grun (1942). We note that if one considered the chain as being composed of $N-1$

https://doi.org/10.1017/S0022112096004302 Published online by Cambridge University Press

N	$\lambda_1^{birefringence}$	λ_1^{stress}
2	0.0841	0.0836
3	0.142	0.127
5	0.411	0.388
10	1.42	1.52
25	9.43	9.35
50	35.5	36.6
100	142	146

TABLE 2. Long relaxation time obtained from birefringence and stress

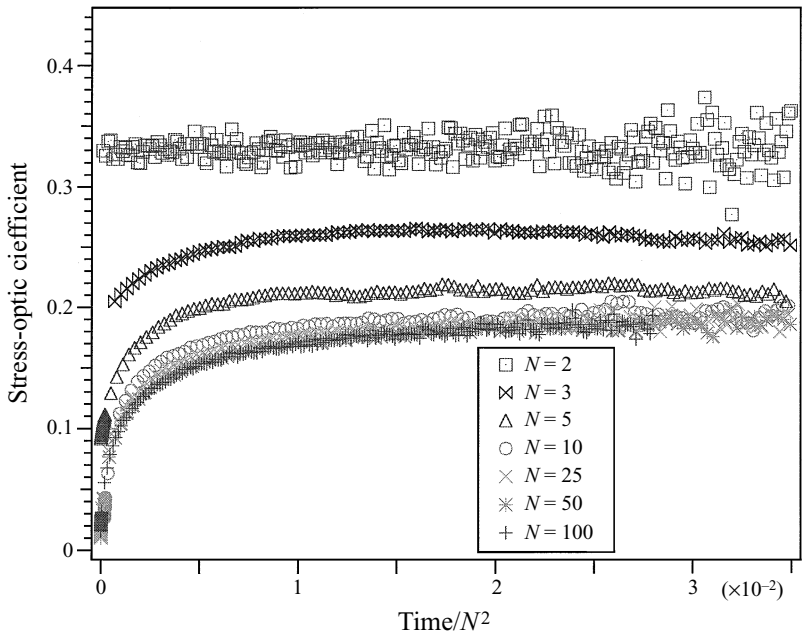


FIGURE 2. Stress-optic coefficient for an initially straight chain aligned in the '1'-direction for $N = 2, 3, 5, 10, 25, 50, 100$.

unconnected dumbbells and used equation (6.1), the coefficient 5 in equation (8.2) would be 3. The stress in a chain exceeds that in a collection of dumbbells due to its connectivity and inextensibility.

The fastest decay process is determined by the smallest rigid length scale in the chain, i.e. the inter-bead separation. Initially in the straight chain the beads will freely diffuse in the transverse direction as if they were $N-1$ rigid dumbbells. The dimensionless rotary diffusivity of a rigid dumbbell is 12 so the birefringence will initially decay as

$$\lim_{t\to 0} \frac{n_{ij}}{N-1} = \mathrm{e}^{-12\,t} \approx 1 - 12\,t\,\ldots \tag{8.3}$$

as seen in figure 3. Grassia & Hinch (1996) found that the stress in a straight chain decays from its value of $\frac{1}{3}kTN^3$ on a time scale of $1/(2.1N^2)$. To obtain this time

https://doi.org/10.1017/S0022112096004302 Published online by Cambridge University Press

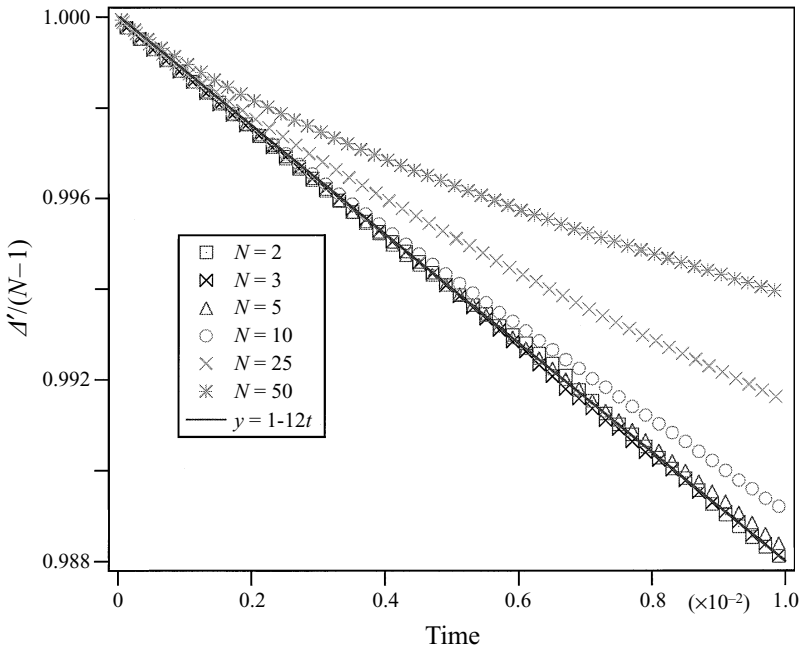


FIGURE 3. Short-time birefringence scaled by $(N-1)$ versus t/N^2 for an initially straight chain aligned in the '1'-direction for $N = 2,3,5,10,25,50,100$. The solid line is the analytic expression for the short-time birefringence decay for a rigid dumbbell.

scale they assume that the beads initially freely diffuse in the directions transverse to the chain alignment. An equivalent initial diffusive motion is obtained by replacing the chain with $N-1$ rigid dumbbells. The different time scale arises because they are considering the decay of initially $O(N^2)$ tensions in the rods which are related to the stress while we base our time scale on only the orientation of a rod, an $O(1)$ quantity.

9. Steady shear flow

In this section we will discuss the steady-state dynamics and rheology of bead–rod chains in simple shear flow

$$u_i^{\infty}(r_i^v) = Pe\,\delta_{i1}\delta_{j2}r_j^v. \tag{9.1}$$

In previous work Liu (1989) calculated the polymer viscosity and first normal stress coefficient for small chains, $N \leqslant 20$. We also calculate these quantities in our simulations, but we examine much larger chains, as well as calculating the birefringence and distinguishing between Brownian and viscous stresses.

The polymer contributions to the shear viscosity and first normal stress coefficient are defined by the relations

$$\eta^p = \frac{\tau_{12}^p}{Pe}, \tag{9.2}$$

$$\Psi_1^p = \frac{\tau_{11}^p - \tau_{22}^p}{Pe^2}. \tag{9.3}$$

https://doi.org/10.1017/S0022112096004302 Published online by Cambridge University Press

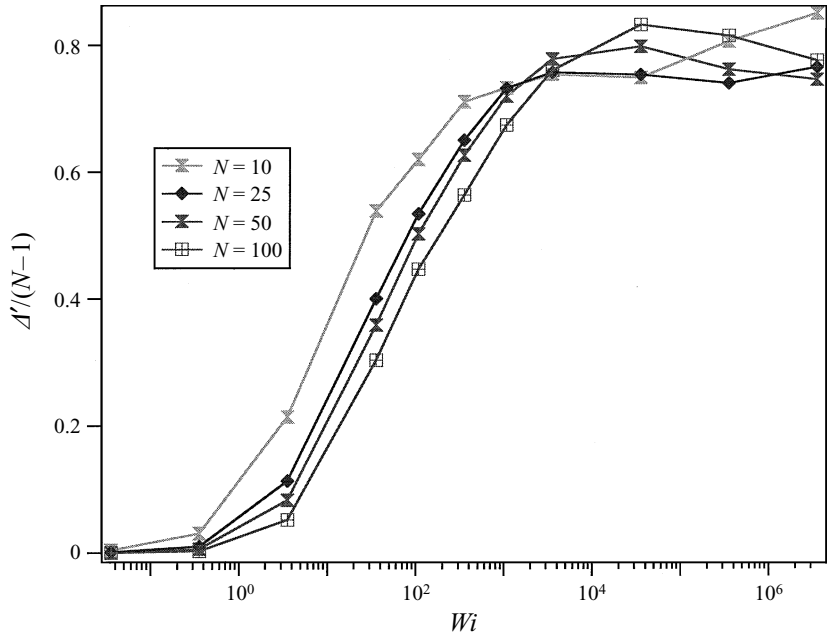


FIGURE 4. Birefringence scaled by $(N-1)$ in shear flow versus Wi for $N = 5, 10, 25, 50, 100$.

Making use of equation (5.12) one can show that at steady state

$$\eta^{p,ss} = \sum_{v=1}^{N} \left\langle \frac{R_2^v R_2^v}{2} \right\rangle, \tag{9.4}$$

$$\Psi_1^{p,ss} = \sum_{v=1}^{N} \left\langle \frac{R_1^v R_2^v}{Pe} \right\rangle. \tag{9.5}$$

Thus polymer configurations having portions of the chain oriented transverse to the mean flow direction contribute most to the shear viscosity while chains tending to align along the line $x_1 = x_2$ contribute most to the first normal stress coefficient.

The steady-state shear viscosity, $\eta^{p,ss}$, as a function of Wi can be roughly separated into three regions: a plateau region for $Wi < 1$ (region I), a power-law region for $1 < Wi < 1000$ (region II) and a second 'weaker' power-law region for $Wi > 1000$ (region III). Each region can be characterized by a distinct change in the chain dynamics giving rise to the rheological behaviour.

In region I, the time to distort the coiled chain from its equilibrium configuration is much larger than the time for the chain to relax due to thermal fluctuations. This is reflected in the relatively small birefringence in figure 4 and a relatively constant value for the viscosity in figure 5 where the viscosity has been scaled with the value for a random walk in the limit $Wi \to 0$ (Bird *et al.* 1987), $(N^2-1)/36$. The flow does cause small perturbations to the coil in the flow direction '1' which scale with Wi. These small perturbations rotate the coil towards the flow direction decreasing the extinction angle, χ, as seen in figure 6 and this results in a constant first normal stress coefficient as seen in figure 7 where Ψ_1^p has been scaled with the value for a random walk in the

https://doi.org/10.1017/S0022112096004302 Published online by Cambridge University Press

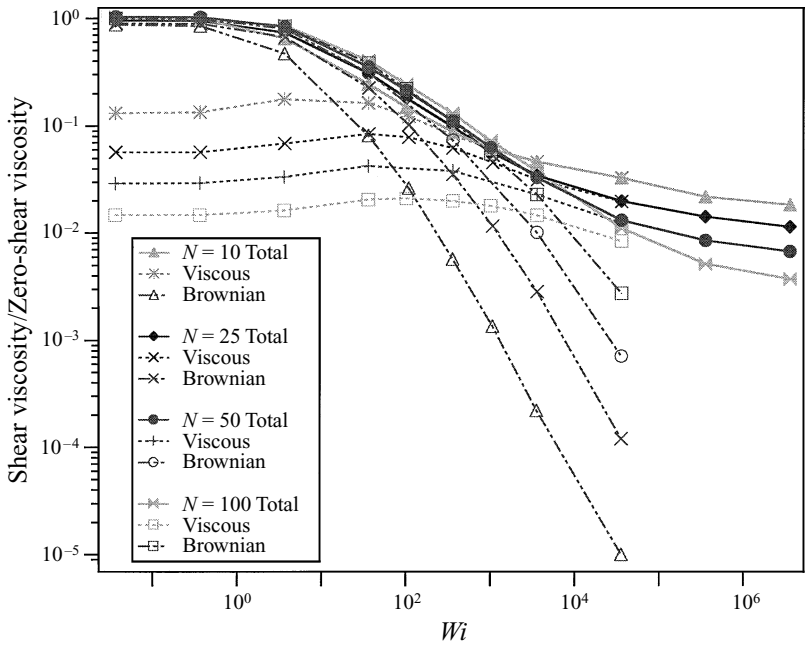


FIGURE 5. Steady-state shear viscosity scaled with the zero-shear value versus Wi for $N = 5, 10, 25, 50, 100$. The viscous and Brownian components are also shown.

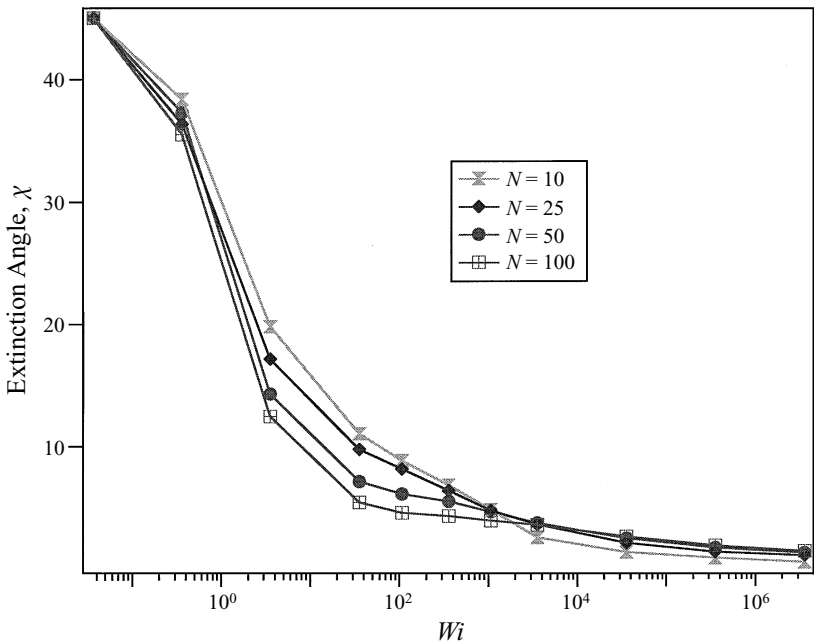


FIGURE 6. Extinction angle in shear flow versus Wi for $N = 5, 10, 25, 50, 100$.

https://doi.org/10.1017/S0022112096004302 Published online by Cambridge University Press

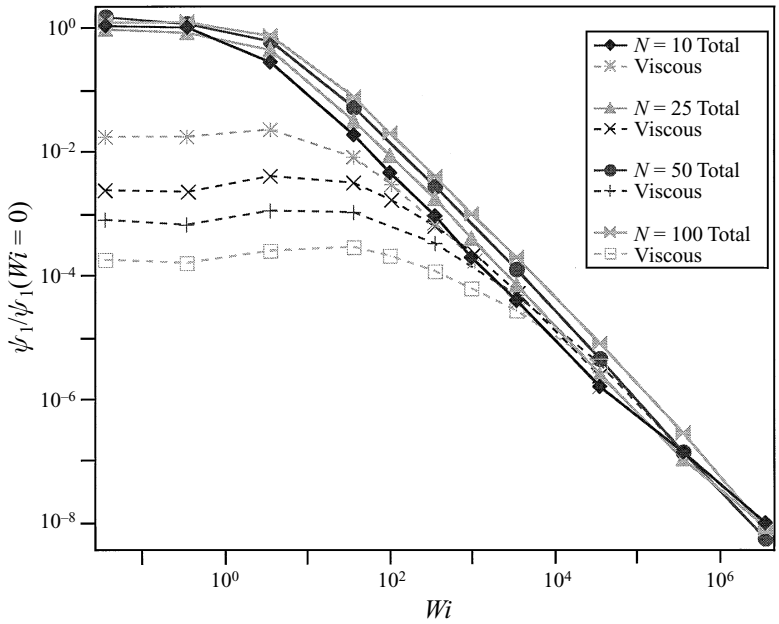


FIGURE 7. Steady-state first normal stress coefficient scaled with the zero-shear value versus Wi for $N = 5, 10, 25, 50, 100$. The viscous component is also shown.

limit $Wi \to 0$ (Bird *et al.* 1987), $2(N^2-1)(10N^3-12N^2+35N-12)/(32400N)$. The relatively small viscous contribution to η^p scales with N, as discussed below, while the total viscosity scales with N^2. Thus as N becomes large the viscous contributions scaled by the total viscosity go to zero. Note for $N = 10$ that the viscous contributions to η^p are only 13% (cf. figure 5). Similarly, the viscous contribution to Ψ_1^p scales with N, while Ψ_1^p scales with N^4 and thus Ψ_1^p becomes purely Brownian as N increases. For $N = 10$ the viscous contributions to Ψ_1^p constitute only 3% of the total value (cf. figure 7).

The $Wi \to 0$ viscous contribution to η^p can be physically understood if we consider the constraints on a chain at equilibrium. As a first approximation, the equilibrium configuration of a bead–rod chain is a random walk. The $Wi \to 0$ viscous constraints are obtained by assuming the chain configuration is unperturbed by the fluid velocity and solving for the constraint forces only considering the hydrodynamic forces (i.e. neglecting Brownian forces). Considering bead v in the chain, the viscous contributions to T^{v-1} and T^v can be approximated by treating the chain as comprising independently aligned dumbbells

$$T^{v-1} = -\tfrac{1}{2}Pe\, u_1^{v-1}u_2^{v-1}, \tag{9.6}$$

$$T^{v} = -\tfrac{1}{2}Pe\, u_1^{v}u_2^{v}. \tag{9.7}$$

The viscous contribution to the shear viscosity from bead v is then

$$\left\langle -\tfrac{1}{2}R_2^v\left(u_1^v u_1^v u_2^v - u_1^{v-1}u_1^{v-1}u_2^{v-1}\right)\right\rangle. \tag{9.8}$$

At equilibrium, $\langle u_1^v u_1^v\rangle = \langle u_1^{v-1}u_1^{v-1}\rangle = 1/3$ and equation (9.8) can be written as

$$\left\langle -\tfrac{1}{6}(r_2^v - r_2^{cm})\left((r_2^{v+1} - r_2^v) - (r_2^v - r_2^{v-1})\right)\right\rangle. \tag{9.9}$$

https://doi.org/10.1017/S0022112096004302 Published online by Cambridge University Press

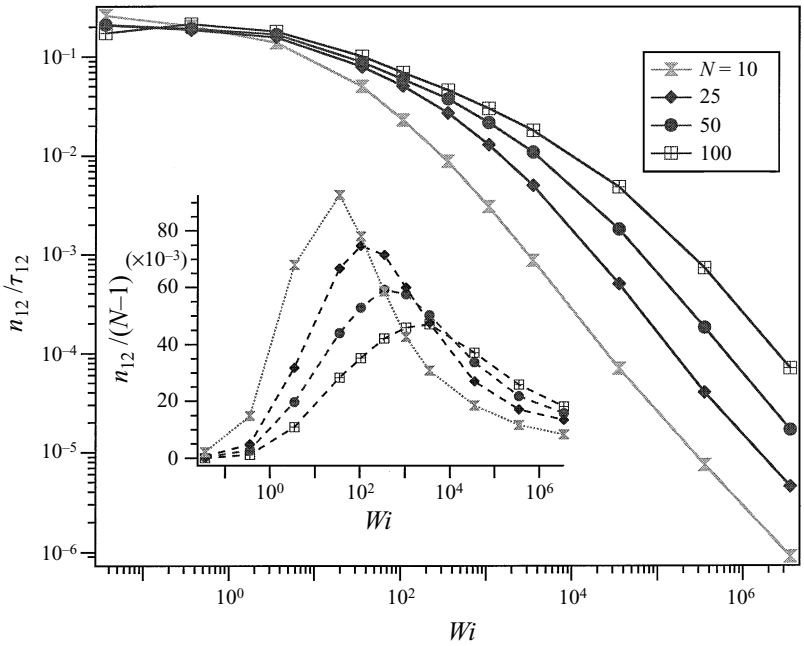


FIGURE 8. Stress-optic coefficient versus Wi for chains in shear flow using the 1,2-component of the stress and index of refraction tensors for $N = 5, 10, 25, 50, 100$. The inset graph shows the index-of-refraction $n_{12}/(N-1)$ versus Wi.

For a random walk with the first bead located at the origin, $\langle r_2^{v+1} r_2^v \rangle = \langle r_2^v r_2^v \rangle = (v-1)/3$ and $\langle r_2^v r_2^{v-1} \rangle = (v-2)/3$ reducing equation (9.9) to

$$\tfrac{1}{18} + \left\langle \tfrac{1}{6} r_2^{cm} \left((r_2^{v+1} - r_2^v) - (r_2^v - r_2^{v-1}) \right) \right\rangle . \tag{9.10}$$

Summing the contributions for N beads gives $\eta^{p,viscous} \approx N/18$ and thus the viscous polymer contribution to the viscosity scales with N. The viscous contribution to the zero shear viscosity in the simulations was best fit to the line $0.0413N - 0.0533$ with a correlation function of magnitude 0.999965. The previous simple scaling also predicts a linear fit but with a slope of 0.0556 (1/18).

Figures 8 and 9 show the stress-optic coefficient based on n_{12} and $n_{11} - n_{22}$ respectively which are shown in the inset figures. For low values of Wi, C reaches a plateau that is independent of N. The low-Wi limiting value of C is approximately 0.2, the same as that obtained in the stress relaxation simulations in figure 2. Since the chain is only slightly stretched relative to its equilibrium configuration and the stress is mostly Brownian, we expect a relatively constant value for C as discussed previously in §7.

In region II, the characteristic flow time is shorter than the chain relaxation time and the chain becomes greatly distorted by the flow. The birefringence in figure 4 steadily increases to nearly 80% of its maximum as a result of the chain being stretched in the flow direction and this value increases with increasing N. The extinction angle, χ, continues to decrease as the chain is rotated in the flow direction, but at a much slower rate than in region I, cf. figure 6. The behaviour of the birefringence and extinction angle suggest that the chain is initially rotated in the flow direction at low Wi in region I and starts to appreciably stretch at much larger Wi in region II. The viscosity and first normal stress coefficient begin to decay at $Wi \approx 1$. The

https://doi.org/10.1017/S0022112096004302 Published online by Cambridge University Press

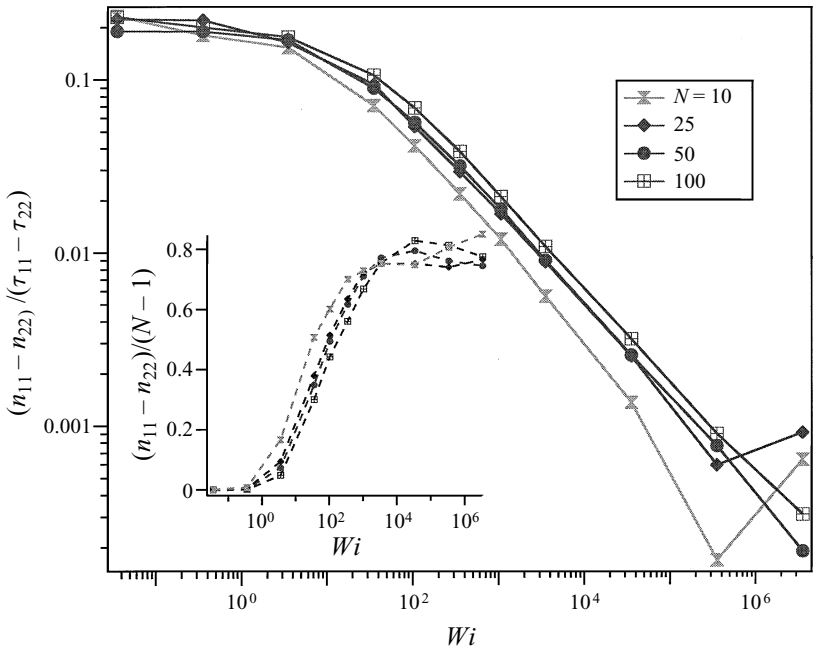


FIGURE 9. Stress-optic coefficient versus Wi for chains in shear flow using the difference in the 1,1 minus the 2,2 component of the stress and index of refraction tensors for $N = 5, 10, 25, 50, 100$. The inset graph shows the difference in the index of refraction components $(n_{11} - n_{22})/(N - 1)$ versus Wi.

viscosity and first normal stress coefficient for different values of N collapse onto single universal curves as shown in figures 10 and 11 respectively. The shear viscosity and first normal stress coefficient power-law thinning is mainly due to the decay of the Brownian stress contribution while the viscous contributions show a slight increase in this region. This increase is due to the chain connectivity and deformation in the flow. As the flow rotates and unravels the chain, the rod orientations become correlated. These orientation correlations necessitate correlated velocities to maintain connectivity of the segments and thus the movement of the chain ceases to be purely affine. This correlated movement coupled with an increasing Wi can explain the slight increase in the viscous contribution to η^p and Ψ_1^p. The subsequent thinning at larger Wi is due to the rotation of the nearly unravelled chain in the flow direction which reduces the velocity gradient of the chain samples. The Brownian and viscous contributions to the viscosity and first normal stress coefficient become comparable in this region as shown in figures 5 and 7. For the largest chain, $N = 100$, the viscous and Brownian contributions to the effective shear viscosity are equal only at a very large value of $Wi \approx 10^4$. The stress-optic law begins to break down in this region due to the large distortions of the chain and the growing viscous contribution to the stress. The stress-optic coefficient now also depends on which components of the index-of-refraction and stress tensors are compared as shown in figures 8 and 9. The stress-optic relation as defined in equation (7.5) is no longer valid and the right-hand side must be replaced by the more general form $C_{ijkl}(Wi)\sigma_{kl}^p$.

We expect that the onset of shear thinning in region II will slowly shift to higher Wi as N increases. If we let N approach infinity at a given Wi, we expect to recover linear viscoelastic behaviour, i.e. the viscosity and first normal stress coefficient will

https://doi.org/10.1017/S0022112096004302 Published online by Cambridge University Press

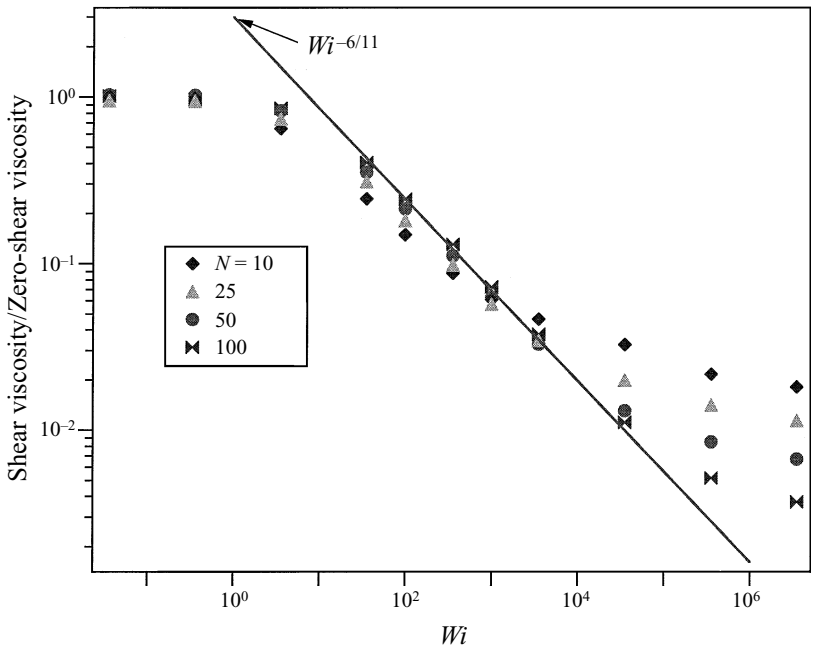


FIGURE 10. Steady-state shear viscosity scaled with the zero-shear value versus Wi for flexible chains and comparison to power law $Wi^{-6/11}$.

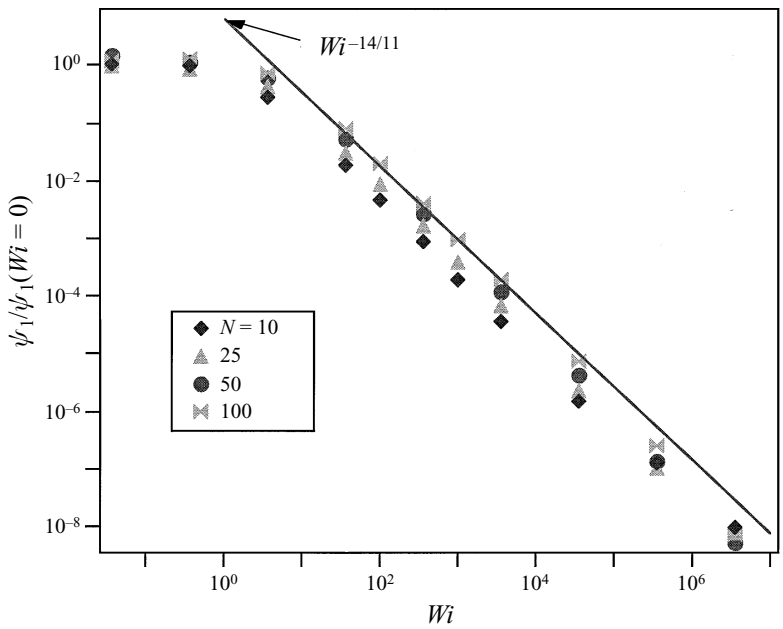


FIGURE 11. Steady-state first normal stress coefficient scaled with the zero-shear value versus Wi and comparison to power law $Wi^{-14/11}$.

https://doi.org/10.1017/S0022112096004302 Published online by Cambridge University Press

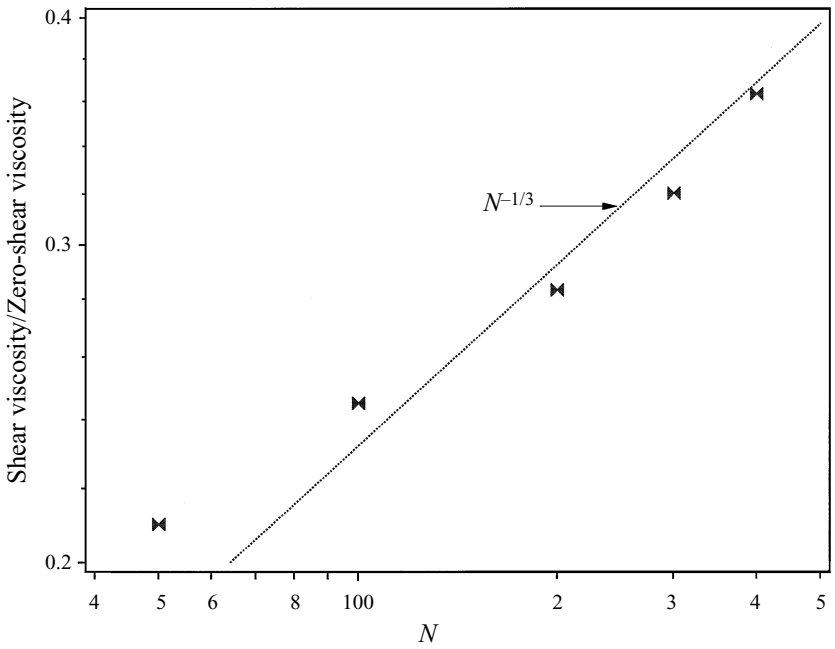


FIGURE 12. Steady-state viscosity scaled with the zero-shear value for $Wi = 100$ versus N and comparison to power law $N^{1/3}$.

gradually approach their zero-shear value. For a FENE-PM (Wedgewood, Ostrov & Bird 1991) bead–spring chain, we can show the analogous behaviour if we consider fixing the FENE parameter b, fixing the chain Wi and analysing the N dependence of the high-Wi power-law behaviour. For large but finite N, it is easy to show that the high-Wi viscosity scaled by the zero-shear value scales with $N^{1/3}Wi^{-1/3}$ and the first normal stress coefficient scaled by the zero-shear value scales with $N^{1/3}Wi^{-4/3}$. In figure 12 we show results for the steady-state shear viscosity of large bead–rod chains for $Wi = 100$. The viscosity gradually increases with increasing N, though for $N = 400$ the viscosity is still substantially less than the zero-shear value, indicating a large amount of shear thinning. The viscosity increase is very close to the slow $N^{1/3}$ increase observed for a FENE-PM chain. Thus, for finite N there will still exist a power-law region in which the viscosity and first normal stress coefficient shear thin, but this will occur at larger Wi as N increases.

The rheology of the chains in region II can be better understood by considering the trajectory of a single chain as shown in figure 13. The chain can be thought of as a string being pulled straight due to the flow forces and undergoing distortions transverse to the average orientation due to Brownian forces. The chain executes 'flips' with a typical breadth in the '2'-direction (or shear gradient direction) which is somewhat greater than one connecting rod length but much smaller than the total length of the chain. From equation (9.4), the viscosity is directly related to the average '2'-component of a bead position relative to the chain centre of mass and is thus related related to the transverse distortions in the chain.

The viscosity scaling can be physically understood by a quasi-steady balance between the tension induced by the flow and the Brownian forces. To understand these tensions, we must first consider the form of the Brownian forces for an extended bead–rod chain in the absence of flow. Recently Grassia & Hinch (1996) have

https://doi.org/10.1017/S0022112096004302 Published online by Cambridge University Press

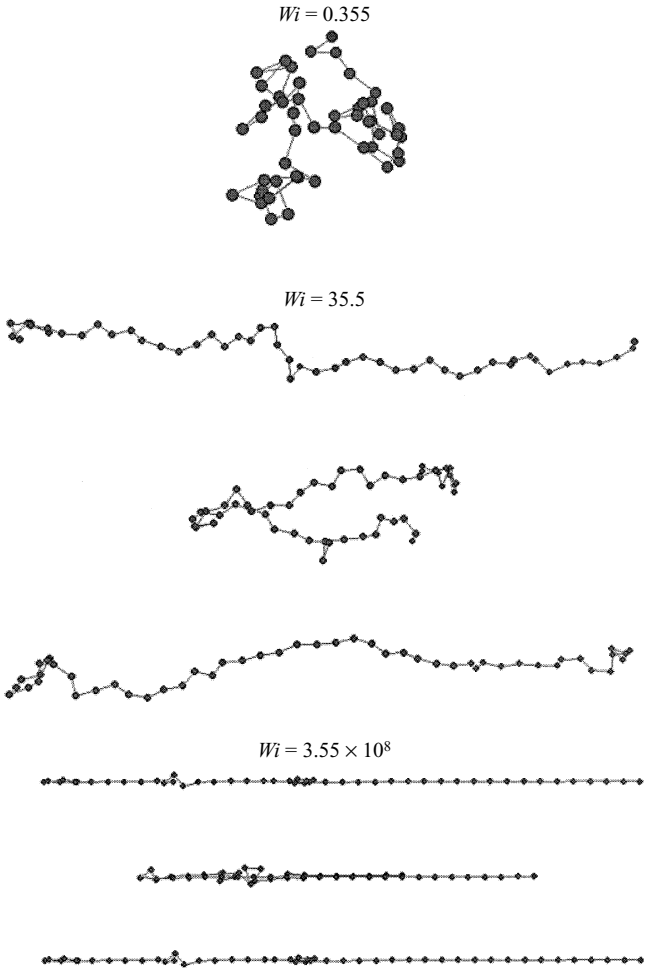


FIGURE 13. Sample chain trajectories in steady shear flow for $N = 50$ and $Wi = 0.355, 35.5$ and 3.55×10^8.

shown that a bead–rod chain which is initially uncoiled and aligned along the '1'-direction will undergo anomalous diffusion, i.e. mean-square displacements which scale nonlinearly with time, in the transverse direction for $1/N^2 < t < N^2$. For $t < 1/N^2$ the average squared distortion grows with t corresponding to free diffusion and with $t^{1/2}$ for $t > 1/N^2$. The anomalous diffusion is due to the constraints and is completely analogous to the anomalous diffusion of small molecules in a confined or constrained geometry (Müller-Plathe, Rogers & Gunsteren 1992). Using our viscosity results for $N = 50$ and 100 and equation (9.4), the mean-squared displacement of a bead in the '2'-direction relative to the centre of mass of the chain is between 1 and 0.01. Assuming that the chain is nearly fully aligned in the flow direction, the average displacement in the '2'-direction is approximately equal to the displacement transverse to the chain orientation. Thus in our discussion we will assume that the chain is exactly aligned in the flow direction and transverse distortions will refer to any displacements in the '2'-direction.

In figure 14 the mean-square transverse displacement relative to the centre of mass of the chain for several beads in a 50-bead chain initially aligned in the '1'-direction

https://doi.org/10.1017/S0022112096004302 Published online by Cambridge University Press

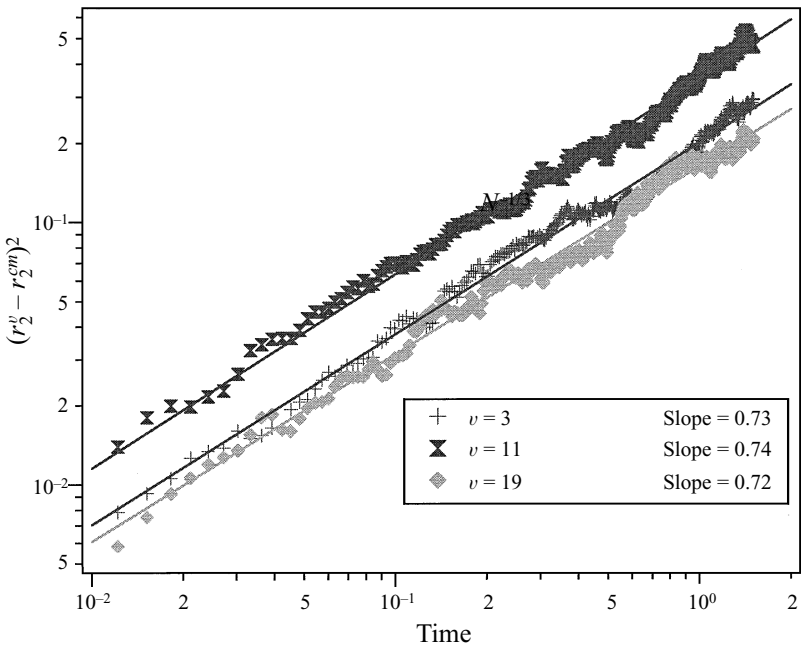


FIGURE 14. Individual bead diffusion in a 50-bead chain initially aligned in the '1'-direction and allowed to relax. The mean-squared transverse displacement in the '2'-direction relative to the chain centre of mass versus time for the 3rd, 11th and 19th bead are shown. The lines are the best fit to the function t^{ρ} where $\rho = 0.73$, 0.74 and 0.72 for $N = 3, 11$ and 19 respectively.

with $Wi = 0$ is shown. We have focused on the range of displacements corresponding to our shear viscosity data. The transverse displacements grow at a rate proportional to t^a where a is approximately 3/4, or with an exponent which is the average of the two time exponents reported by Grassia & Hinch (1996). The diffusive process can then be expressed as

$$\langle R_2^v R_2^v \rangle = D(R_2^v)t, \tag{9.11}$$

$$D(R_2^v) = (R_2^v)^{-2/3}. \tag{9.12}$$

Physically this corresponds to a diffusivity which decreases as R_2^v increases due to the rotation of the connecting rods into the transverse direction. The constraints specify that the velocity of a rod must be perpendicular to its orientation which is maintained by applying constraint forces with an orientation parallel to the rods. The constraint forces tend to decrease the effective Brownian force in the direction of the rod orientation.

The shear flow gives rise to tensions in the chain which scale with PeR_2^v. The magnitude of the transverse Brownian forces can be estimated as $(D(R_2^v))^{1/2}/t$, or from equation (9.12) is of order $(R_2^v)^{-8/3}$. If we assume the tension due to the flow is balanced by the Brownian tension, then $R_2^v \propto Pe^{-3/11}$. Thus we expect the breadth of the chain in the '2'-direction to scale with $Pe^{-3/11}$. Due to the flexible nature of the chain, the chain will also flip within a distance from the '1'-axis that obeys the $Pe^{-3/11}$ scaling. The chain thus contributes an order-$Pe^{-6/11}$ amount to the viscosity when it flips and an order-$Pe^{-6/11}$ amount afterwards, resulting in a viscosity which scales with $Pe^{-6/11}$. Our simulations compare favourably to the predicted $Pe^{-6/11}$ scaling as shown in figure 10.

https://doi.org/10.1017/S0022112096004302 Published online by Cambridge University Press

Using equation (9.5), the previous scaling for R_2^v and an expected $O(1)$ value for R_1^v, the first normal stress coefficient is predicted to scale with $Pe^{-14/11}$. The decrease of Ψ_1^p is similar to the $Pe^{-4/3}$ decrease for a single rigid rod (Hinch & Leal 1972). The rigid rod spends most of its time aligned in the flow direction in a region of order $Pe^{-1/3}$ where diffusion and advection are comparable. We note that previously Liu (1989) observed a $Pe^{-1/2}$ power-law decrease for η^p and a $Pe^{-4/3}$ power-law decrease for Ψ_1^p for small bead–rod chains, though no physical explanation for the exponents was given.

In region III, the average transverse displacement of the chain becomes much smaller than the rod size (i.e. $Pe^{-3/11} \ll 1/(N-1)$). Most of the chain is aligned in the flow direction, but due to Brownian fluctuations, portions of the chain are flipping. The smallest 'flipping event' that can occur is the rotation of an individual rod which results in displacements in the '2'-direction which are much larger than those in the straight portions of the chain as shown in figure 13. The chain is continually flipping and often does not completely extend to its full length before starting to flip again. The displacements due to flipping dominate the viscosity and first normal stress coefficient. The viscosity, figure 5, has nearly a plateau value because the transverse displacements during flipping are governed by the smallest rigid length scale, the connecting rods. By contrast, the first normal stress coefficient in figure 7 shows a slightly larger power-law decay due to the chain not extending fully before flipping. The dynamics is also reflected in the birefringence which reaches a plateau value near 80% of its maximum value while the extinction angle slowly continues to decrease as the straight regions of the chain rotate closer to the '1'-axis.

In addition to the equilibrium osmotic pressure contribution by the polymer $n_p kT$, their is a *dynamic* polymer pressure:

$$P^{p,dyn} = -\tfrac{1}{3}\tau_{ii}^p \tag{9.13}$$

The dynamic polymer pressure arises solely due to the flow and is zero at equilibrium. At steady state we can make use of the Giesekus form of the stress tensor and the dimensionless pressure ($P^{p,dyn}/n_p kT$) can be written as

$$P^{p,dyn} = -\tfrac{1}{6}Pe\sum_{v=1}^{N}\langle \kappa_{ik}R_k^v R_i^v + R_i^v R_k^v \kappa_{ki}^{\dagger}\rangle \tag{9.14}$$

In linear shear flow this becomes

$$P^{p,dyn} = -\tfrac{1}{3}Pe\sum_{v=1}^{N}\langle R_1^v R_2^v\rangle. \tag{9.15}$$

We note that this is equal to $-Pe^2\Psi_1^p/3$. In steady extensional flow the dynamic pressure is

$$P^{p,dyn} = -\tfrac{1}{3}Pe\sum_{v=1}^{N}5\langle R_1^v R_1^v - 0.5R_2^v R_2^v - 0.5R_3^v R_3^v\rangle. \tag{9.16}$$

The dimensionless dynamic polymer pressure for a Hookean dumbbell in shear flow is (Bird *et al.* 1987)

$$P_{Hookean}^{p,dyn} = -\tfrac{2}{3}Wi^2 \tag{9.17}$$

and in extensional flow for $Wi < 1$ is

$$P_{Hookean}^{p,dyn} = -\left[\frac{1-0.5Wi}{(1+0.5Wi)(1-Wi)}\right] + 1. \tag{9.18}$$

https://doi.org/10.1017/S0022112096004302 Published online by Cambridge University Press

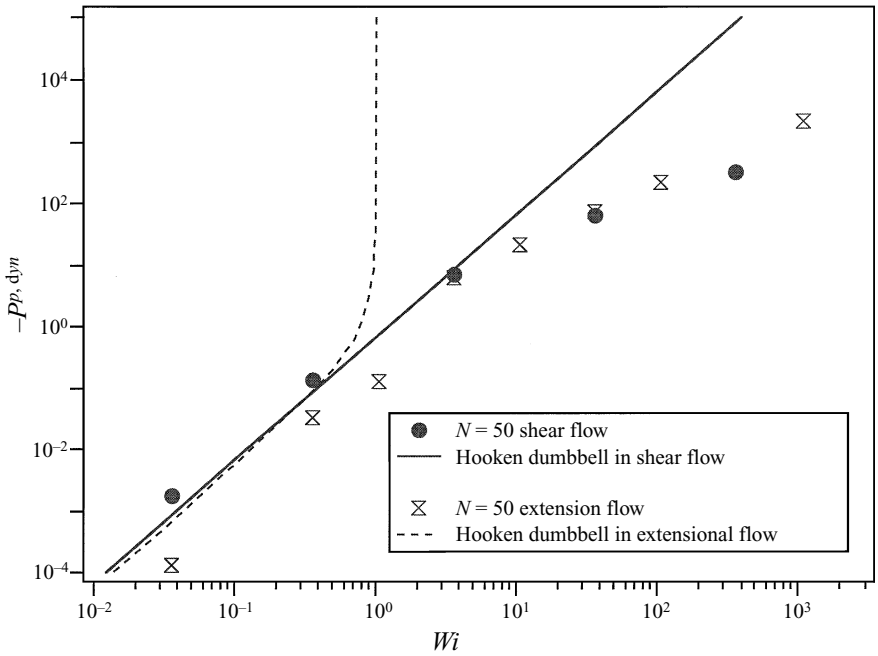


FIGURE 15. Steady-state dynamic polymer pressure verses Wi in shear and extensional flow for a 50-bead chain and a Hookean dumbbell.

In figure 15 we show the dynamic polymer pressure for $N = 50$ in shear and extensional flow along with the results for a Hookean dumbbell. Note that the magnitude of the dynamic pressure for both models increases with increasing Wi, and the pressure is negative. If we consider the chain as a collection of beads, attractive forces between beads tend to lower the osmotic pressure while repulsive forces, such as hard-sphere repulsions, will lead to increases in the osmotic pressure. Collectively, the rods in the bead–rod model, and also the spring in the Hookean dumbbell act to resist changes from the equilibrium chain configuration. In shear and extensional flows they act as attractive forces which will decrease the dynamic polymer pressure as Wi increases. This is in accord with the non-equilibrium molecular dynamics of bead–spring chains of Kröger, Loose & Hess (1993) in which a decrease in the pressure is attributed to intramolecular bond stretching. In figure 15, the bead–rod $P^{p,dyn}$ compares favourably with the Hookean dumbbell for small Wi but deviates at large Wi due to the finite length of the bead–rod chain. The apparent kink in the bead–rod $P^{p,dyn}$ in extensional flow at around $Wi = 1$ is due to the coil-stretch transition in the chain which for a Hookean dumbbell results in a divergence of the microstructure and pressure. At large Wi in extensional flow, the bead–rod chain will reach near full extension and $P^{p,dyn}$ scales with Wi. However, at large Wi in shear flow we have already shown that Ψ_1^p scales with $Wi^{-14/11}$, so $P^{p,dyn}$ will scale with $Wi^{8/11}$. The existence of a non-zero dynamic pressure has been suggested to be the source of concentration gradients which can occur in curvilinear shearing flows (Doi 1990; Milner 1991). The bead–rod chain would predict qualitatively and quantitatively similar trends for the concentration gradients as a Hookean dumbbell at low Wi, but have a smaller affect at large Wi due to a smaller dynamic pressure.

https://doi.org/10.1017/S0022112096004302 Published online by Cambridge University Press

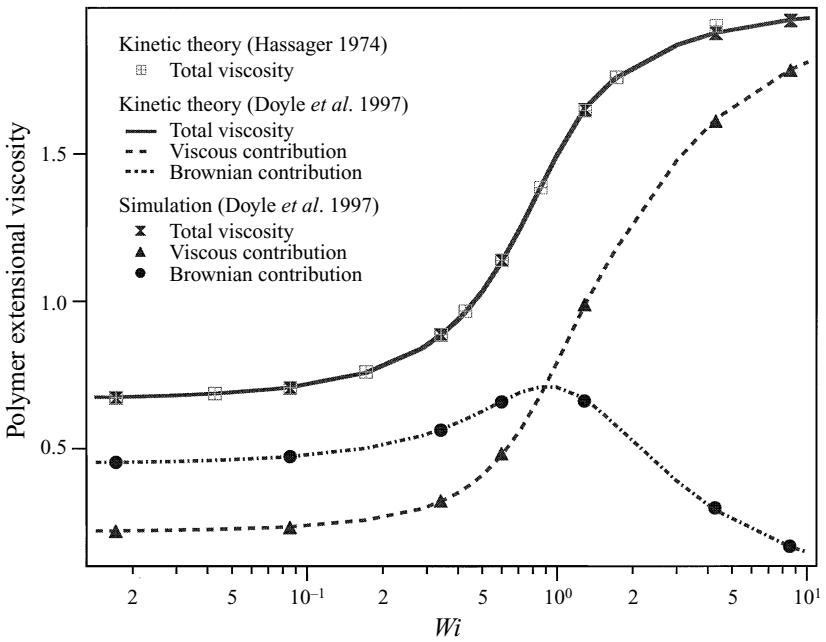


FIGURE 16. Steady-state total, Brownian and viscous extensional polymer viscosity versus Wi for $N = 3$.

10. Steady uniaxial extensional flow

The dynamics and rheology of chains in uniaxial extensional flow:

$$u_i^{\infty}(r_i^v) = Pe\left[\delta_{i1}\delta_{j1} - \tfrac{1}{2}(\delta_{i2}\delta_{j2} + \delta_{i3}\delta_{j3})\right] r_j^v \tag{10.1}$$

has also been examined. The polymer contribution to the extensional viscosity is defined by the relation

$$\eta^p = \frac{\tau_{11}^p - \tau_{33}^p}{Pe}. \tag{10.2}$$

Uniaxial extensional flow is one type of potential flow. The steady-state distribution function, Ψ, for a chain in a potential flow is (Kramers 1946)

$$\Psi = cC^{1/2}\exp(\phi/kT) \tag{10.3}$$

where $\phi = (\xi/2\kappa_{ij})\sum_{v=1}^{N} R_i^v R_j^v$, C is the determinant of a transformation matrix (Hassager 1974) and c is a normalization constant. The average of an arbitrary function $A(R_i^v)$ is then the product of the function and Ψ integrated over the configuration space of the chain. Previously, Hassager (1974) numerically calculated the extensional viscosity for a chain with $N = 3$. Following the method of Hassager (1974), we have calculated the viscous and the Brownian contributions to the polymer extensional viscosity in addition to the total polymer viscosity (the details of this calculation can be found in the Appendix). In figure 16 our simulation and kinetic theory results are shown along with the results of Hassager (1974). We see excellent agreement between our results and Hassager's for the total viscosity, and our kinetic theory and simulations also show excellent agreement. As N becomes large, the computational

https://doi.org/10.1017/S0022112096004302 Published online by Cambridge University Press

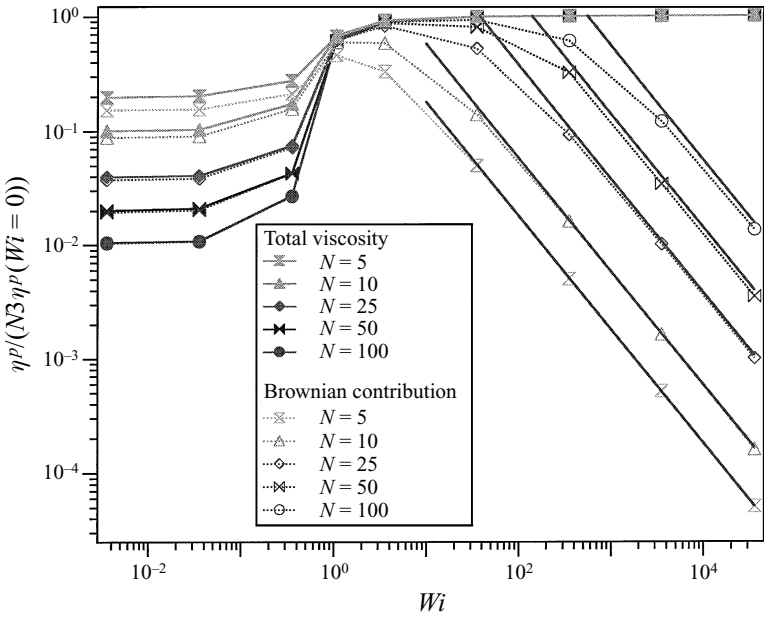


FIGURE 17. Steady-state extensional viscosity and Brownian contribution scaled by $N3\eta^p(Wi \to 0)$ versus Wi for $N = 5, 10, 25, 50, 100$.

time to evaluate the integrals involved in the kinetic theory becomes large and the stochastic simulations are a more feasible means of performing the calculations.

Using asymptotic expansions in Pe, Hassager (1974) developed expressions for the steady-state extensional viscosity for bead–rod chains at low and high extension rates:

$$\eta^p = \begin{cases} \left(1 + \frac{1}{90}Pe\right)\ 3\eta^p(Pe \to 0), & Pe \to 0 \\ \left(1 - (24/N^2Pe)\right)\ N3\eta^p(Pe \to 0), & Pe \to \infty \end{cases} \tag{10.4}$$

where $\eta^p(Pe \to 0)$ is the shear viscosity for a flexible bead–rod chain in the limit that Pe goes to zero or *zero-shear viscosity*. Previous work by Liu (1989) has confirmed these scalings. Using the relaxation time scaling ($\lambda_1 \propto N^2$) and λ_1 for $N = 100$, we can estimate $Wi = 0.0142\, N^2\, Pe$ for large N and write equation (10.4) as

$$\eta^p = \begin{cases} (1 + 0.78Wi)\ 3\eta^p(Pe \to 0), & Wi \to 0 \\ \left(1 - 0.34/Wi\right)\ N3\eta^p(Pe \to 0), & Wi \to \infty\ . \end{cases} \tag{10.5}$$

Thus by scaling the extension rate with the chain time scale λ_1, the extensional viscosity at small and large Wi can be collapsed onto a universal curve for all N. The viscosity will start to appreciably increase at $O(1)$ values of Wi and reach 90% of its maximum value at $Wi = 3.4$.

Figure 17 shows the total polymer extensional viscosity and Brownian contribution versus Wi. The viscous contribution is shown in figure 18 along with the Brownian contribution versus Wi for the three longest chains simulated. In figures 17 and 18 the polymer viscosity has been scaled with $N(N-1)^2/12$ such that the total polymer extensional viscosity asymptotes to 1 for large Wi. At small Wi, η^p is equal to three times the zero shear value. In addition, the viscous and Brownian contributions equal three times their zero-shear-rate value. The low-$Wi\eta^p$ is 76.8% Brownian for $N = 5$ and 98.5% for $N = 100$. At small Wi ($Wi \leqslant 3$) the birefringence in figure 19

https://doi.org/10.1017/S0022112096004302 Published online by Cambridge University Press

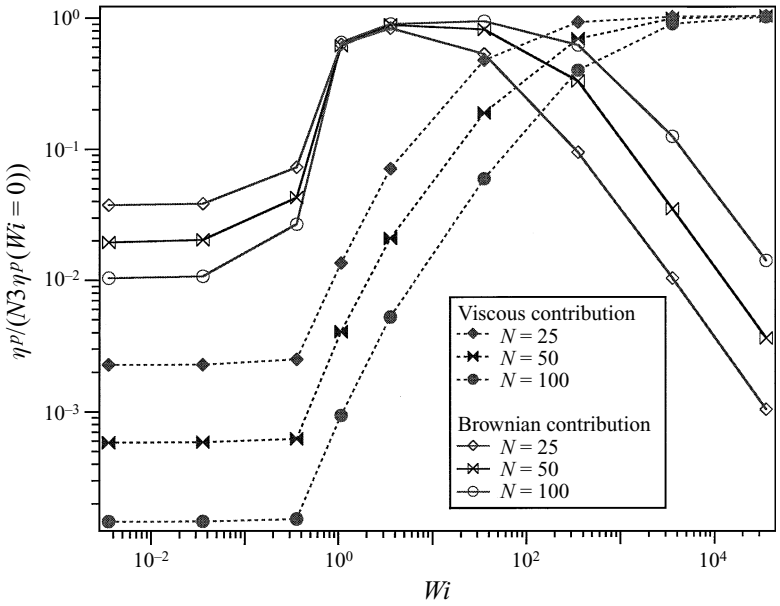


FIGURE 18. Viscous and Brownian contribution to the steady-state extensional viscosity scaled by $N3\eta^p(Wi \to 0)$ versus Wi for $N = 25, 50$ and 100.

approaches zero while the stress-optic coefficient is a constant, independent of N, at a value of $C \approx 0.2$. This is in agreement with the zero-shear and long time relaxation value of C.

At $Wi \approx 1$, the birefringence and viscosity increase rapidly and the stress-optic coefficient begins to decrease. At $Wi = 1.07$, the viscosity is 68.9% Brownian for $N = 5$ and 99.9% for $N = 100$. As N increases, the polymer viscosity in this region becomes increasingly Brownian. Note that even though the viscosity for $N \geqslant 25$ is nearly all Brownian, the stress-optic law fails due to correlations in the connecting rods which give rise to $O(N^3)$ Brownian stresses as discussed previously in §6.

At large Wi the polymer viscosity and birefringence level off as the chain becomes completely unravelled and aligned along the extensional axis. The stress-optic coefficient decreases like Wi^{-1} as a consequence of the plateau in the viscosity and birefringence. The polymer viscosity at 90% of its maximum, $Wi = 3.4$, becomes increasingly Brownian dominated with increasing N. As the chain becomes fully aligned, the Brownian stress levels off to the value given by equation (6.6) shown in figure 17 as solid lines. Eventually the viscous contributions exceed the Brownian, but this does not occur until values of Wi that are quite large. For $N = 100$, the contributions are approximately equal at $Wi = 500$.

The growth of the Brownian contributions with increasing N at large Wi can be understood by examining Hassager's expansions in conjunction with our equation for the Brownian stress from a fully aligned chain. Consider the viscosity at 90% of its maximum, $Wi = 3.4$. We can estimate the Brownian stress as $N^3/3$ using equation (6.6) while the viscous stress in a fully aligned chain is $N^3Pe/12$ or equivalently $5.9NWi$. We will use these limiting forms as an estimate of their magnitude when the chain is nearly fully extended. At $Wi = 3.4$, the viscous contribution is $20N$ while the Brownian is $N^3/3$, giving a ratio of Brownian to viscous contributions of $N^2/60$. Thus the Brownian stresses will become increasingly dominant over the viscous stresses for

https://doi.org/10.1017/S0022112096004302 Published online by Cambridge University Press

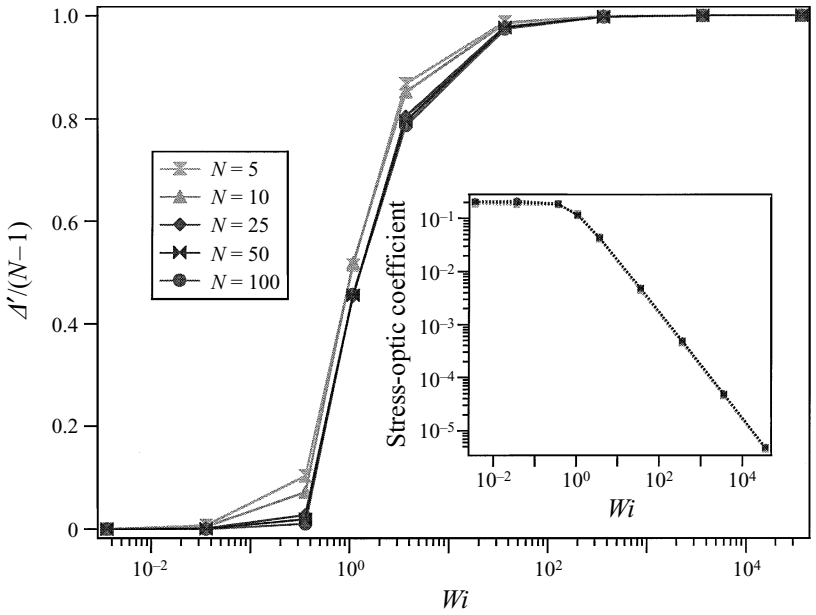


FIGURE 19. Steady-state extensional birefringence scaled by $(N-1)$ versus Wi for $N = 5$, 10, 25, 50, 100. The inset graph shows the stress-optic coefficient versus Wi.

increasing N as seen in figure 18. This can be more easily seen if we plot the ratio of the Brownian contribution to the viscosity divided by the viscous contribution at $Wi = 3.4$ and scale this ratio with N^2 as shown in figure 20. The ratio approaches a constant value of approximately 0.0172 at large N compared to the predicted value of 0.0167 (1/60). Furthermore, the previous scalings can be utilized to show that the viscous and Brownian contributions will be equal at $Wi \approx 0.06N^2$.

Previous work by Hinch (1994*b*) concluded that the transient extensional polymer viscosity for bead–rod chains in strong extensional flow was mainly viscous. For $N = 100$, Hinch assumed that $Pe = 0.2$ ($Wi = 28.4$) constituted a strong flow. Our simulations suggest this is a strong flow in the sense that the polymer configuration is greatly distorted from its equilibrium configuration, but the steady-state stresses remain mostly Brownian. While we have calculated both steady-state values and transient values for the stress, our conclusions differ from Hinch's primarily due to the different algorithms used to calculate the stress. Our algorithm explicitly separates the Brownian from the viscous contributions and avoids order $(\delta t)^{-1/2}$ errors. Hinch does suggest in his work that the small Brownian stresses could be wrong due to his algorithm (Hinch 1994*b*). We have performed preliminary transient simulations confirming that the transient stresses are also Brownian dominated over approximately the same range of Wi as the steady-state values. Figure 21 shows the transient (start-up and decay after flow stopped) total, Brownian and viscous extensional viscosity for $N = 50$ and $Wi = 35$. The dashed lines are the steady-state values from figures 17 and 18. The transient extensional viscosity is mostly Brownian over the full time scale and approaches the steady-state value for long times. Thus the major conclusion of this section is that the extensional viscosity for large flexible bead–rod chains is Brownian dominated until $Wi \gg 1$, i.e. $O(100–500)$, in contrast to previously published results (Hinch 1994*b*). We are currently preparing a more complete study of bead–rod chains in transient flows (Doyle, Shaqfeh & Gast 1997).

https://doi.org/10.1017/S0022112096004302 Published online by Cambridge University Press

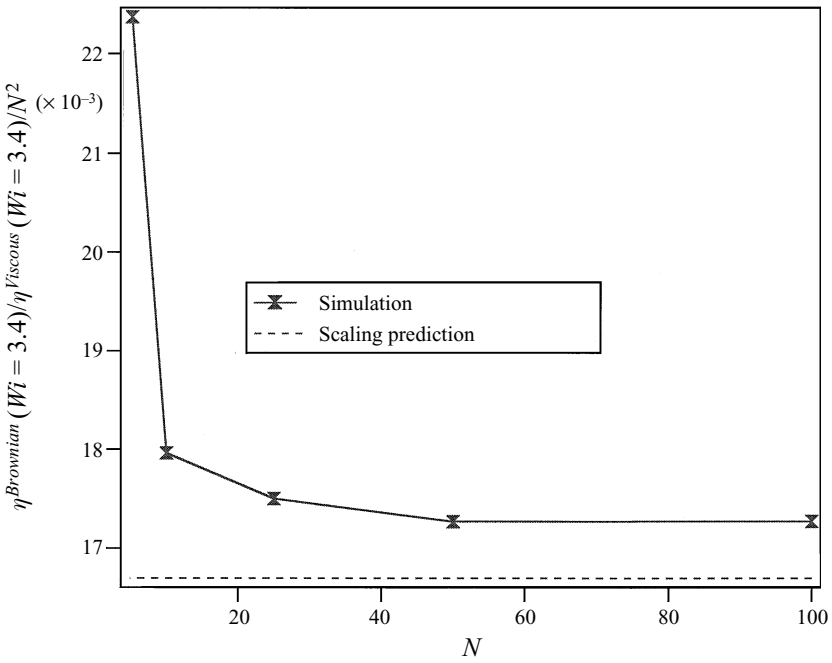


FIGURE 20. The ratio of the Brownian to the viscous contribution to extensional viscosity scaled by N^2 for $Wi = 3.4$ versus N. The line is the scaling prediction 1/60.

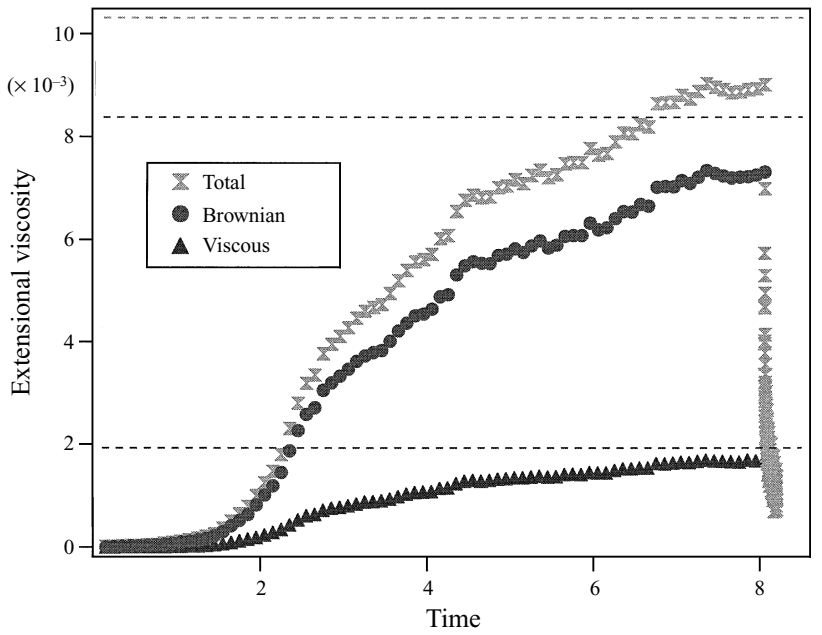


FIGURE 21. The transient total, viscous and Brownian extensional viscosity for $N = 50$ and $Wi = 35.5$ versus time.

https://doi.org/10.1017/S0022112096004302 Published online by Cambridge University Press

11. Comparison to the FENE dumbbell model

The bead–rod chain is often the simplest model one can utilize to determine the statistical mechanics of polymers (Flory 1989), but may be too cumbersome for understanding the rheology of suspensions in complex geometries (Talwar & Khomami 1995). A simpler model is a bead-spring dumbbell where the spring represents an entropic restoring force and the beads act as sources of friction. In this section we will briefly review the derivation of the FENE dumbbell force law, describe a simple Brownian dynamics algorithm for FENE dumbbells and then compare our results for bead–rod chains to Brownian dynamics simulations of FENE dumbbells.

Early work in modelling the physics of polymer solutions done by Kuhn (1934) and by Guth & Mark (1934) consisted of representing a polymer by a random walk of $N-1$ links of length a. The probability distribution function for the chain end-to-end separation is proportional to the number of allowed configurations (given an end-to-end separation distance) and is a Gaussian function. Kuhn & Grun (1942) showed that the magnitude of the force required to hold the ends of the chain at a distance Q apart is given by

$$F_i = \frac{Q_i}{Q}\frac{kT}{a}\mathscr{L}^{-1}\left(\frac{Q}{(N-1)a}\right), \tag{11.1}$$

where $\mathscr{L}^{-1}$ is the inverse Langevin function and Q_i is a vector directed from one chain end to the other. Warner (1972) derived a simpler empirical form for the entropic force:

$$F_i^{FENE} = \frac{3kT}{(N-1)a^2}Q_i \Bigg/ \left[1-\left(\frac{Q}{(N-1)a}\right)^2\right] \tag{11.2}$$

referred to as the Finitely Extensible Nonlinear Elastic spring law or FENE.

We can test the force law directly by performing simulations where we hold a Kramers chain with its ends separated by a given distance Q. Since the reference frame is arbitrary, we fix one chain end at the origin and the other at a position Q located along the '1'-axis. We set Wi to zero and calculate the average force required to hold the end points fixed. Due to the geometry we are considering, the '1'-component of the average force is the only non-zero component. An equivalent spring force for the Kramers chain is then equal to the negative of the average restraining force. In figure 22 we see that the simulations, FENE force law and the inverse Langevin function show good agreement for chains extended less than 50% of their maximum length. For larger extensions the FENE force law predicts smaller forces than the inverse Langevin function and the simulations are well described by the latter. We see that a chain consisting of only 10 beads does an adequate job of capturing the universal scaling for the force-extension curve.

To test the FENE model in non-equilibrium situations, we performed Brownian dynamics simulations for chains with 2 beads joined by a FENE spring in both steady shear and uniaxial extensional flow. The Brownian force on a bead has the following statistics:

$$\langle F_i^{br,v}(t)\rangle = 0, \tag{11.3}$$

$$\langle F_i^{br,v}(t)F_j^{br,\mu}(t')\rangle = 2kT\zeta\ \delta_{v\mu}\ \delta_{ij}\ \delta(t-t'), \tag{11.4}$$

https://doi.org/10.1017/S0022112096004302 Published online by Cambridge University Press

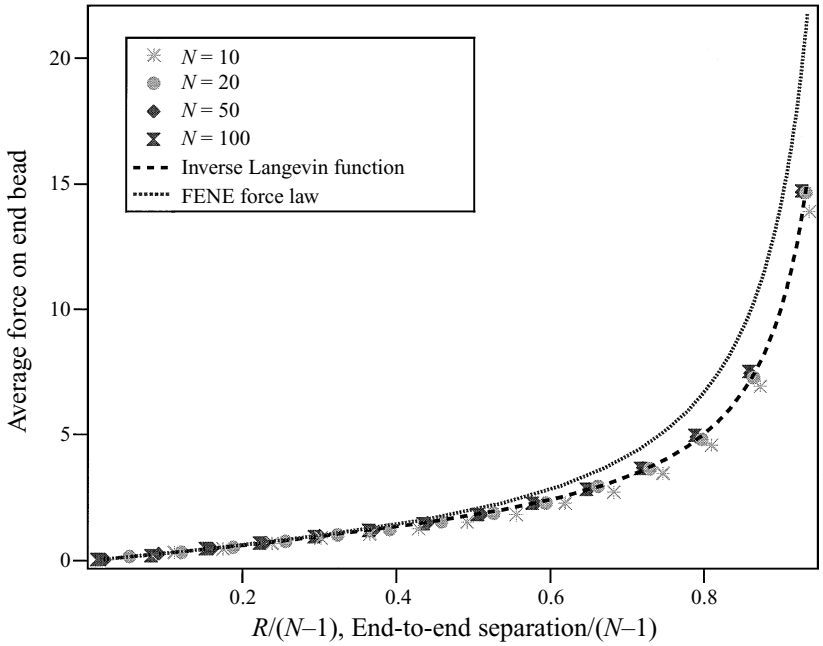


FIGURE 22. The average force required to hold the ends of a bead–rod chain at a fixed separation versus the separation distance for $N = 10$, 20, 50 and 100. The FENE force law and inverse Langevin function are shown for comparison.

where ζ is the drag on a bead with a diameter d. The hydrodynamic force is

$$F_i^{h,v} = -\zeta(\dot{r}_i^v - u_i^\infty(r_i^v)). \tag{11.5}$$

The spring force exerted on bead 2 is chosen to be F_i^{FENE} and on bead 1 is $-F_i^{FENE}$.

The size of a bead is chosen to be half the length of the bead–rod chain or $d = Na/2$. The only parameter in the FENE dumbbell not having a direct relation to a bead–rod chain is ζ. We use ζ as an adjustable parameter to fit the FENE dumbbell to the zero-shear-rate viscosity of the bead–rod chain. We non-dimensionalize the problem by scaling lengths with d and forces with kT/d. This scaling results in a FENE Péclet number, Pe^{FENE}, equal to $\zeta d^2\dot{\gamma}/kT$ (or $\zeta d^2\dot{\epsilon}/kT$). The characteristic relaxation time for the FENE dumbbell, $\zeta d^2(N-1)/(3N^2kT)$ (Bird *et al.* 1987), is used to define a Weissenberg number, Wi^{FENE}, equal to $Pe^{FENE}(N-1)/(3N^2)$. With this assumption, we can now compare our bead–rod chains to an *equivalent* FENE dumbbell. The Brownian dynamics simulations were performed using a simple first-order algorithm and the dumbbell stress was calculated via equation (5.3).

We compare simulations using our longest bead–rod chains, $N = 100$, to the equivalent FENE dumbbell and express the FENE dumbbell results in terms of the bead–rod length scale a. The drag coefficient ζ has been set at $33.625N\xi$ which we note is approximately 2/3 of the drag on half the bead–rod chain. In figure 23 the polymer shear viscosity, made dimensionless with $n_p\xi a^2$, is plotted versus Wi or Wi^{FENE}. The FENE dumbbell does a fair job of qualitatively and quantitatively modelling the bead–rod chain for $Wi < 10^4$. The FENE dumbbell viscosity is proportional to $Wi^{-2/3}$ (Larson 1988) for large Wi while the bead–rod chains have a viscosity proportional to $Wi^{-6/11}$ for intermediate Wi and a much smaller power-law exponent for large Wi. We do not expect the FENE dumbbell to be able to capture the high-Wi viscosity

https://doi.org/10.1017/S0022112096004302 Published online by Cambridge University Press

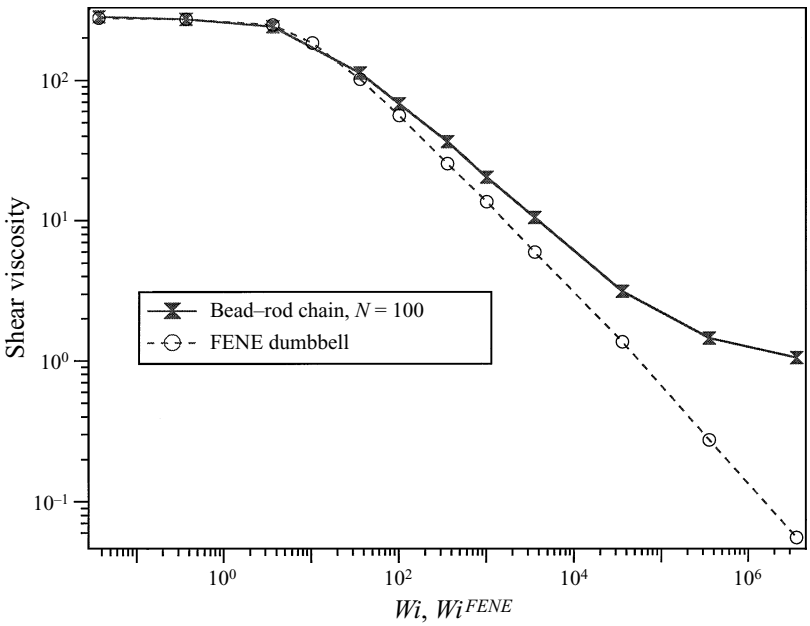


FIGURE 23. The dimensionless polymer shear viscosity versus Wi or Wi^{FENE} for a bead–rod chain with $N = 100$ and the equivalent FENE dumbbell.

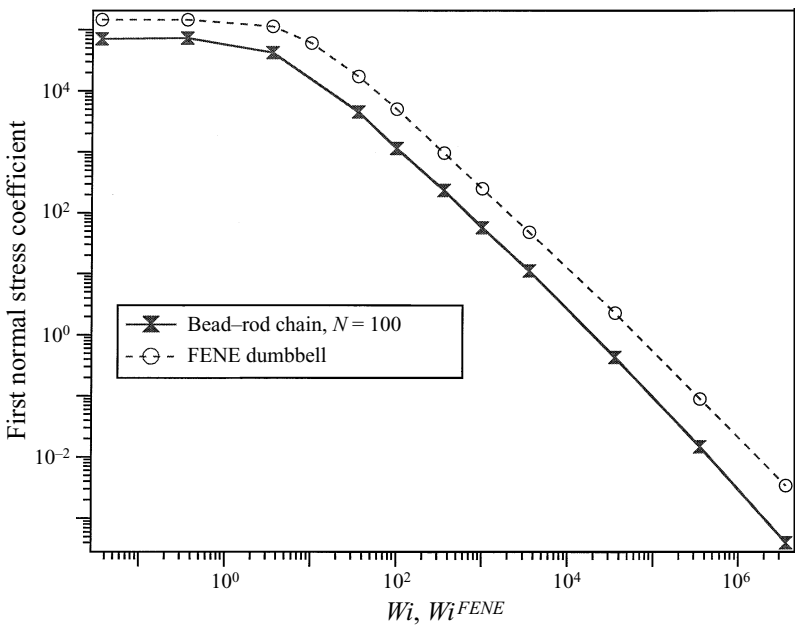


FIGURE 24. The dimensionless polymer shear first normal stress coefficient versus Wi or Wi^{FENE} for a bead–rod chain with $N = 100$ and the equivalent FENE dumbbell.

https://doi.org/10.1017/S0022112096004302 Published online by Cambridge University Press

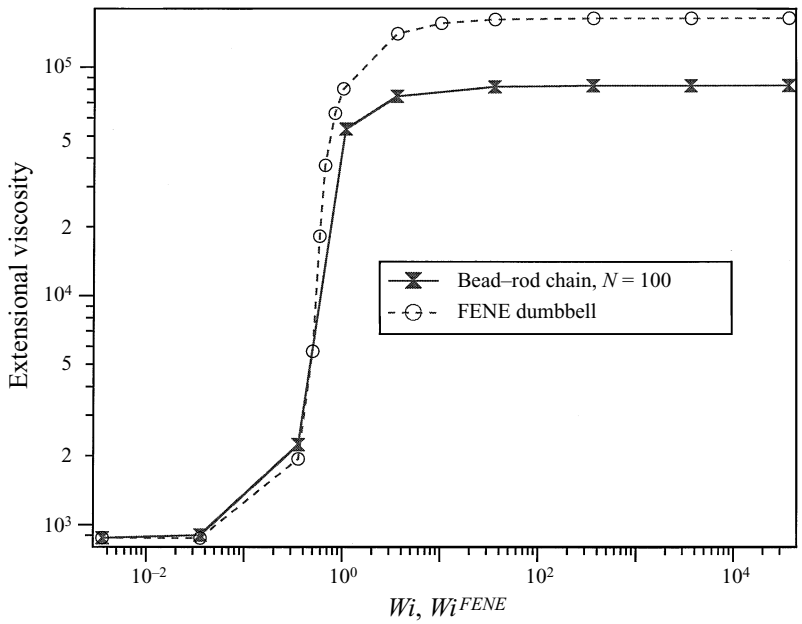


FIGURE 25. The dimensionless polymer extensional viscosity versus Wi or Wi^{FENE} for a bead–rod chain with $N = 100$ and the equivalent FENE dumbbell.

behaviour of a bead–rod chain since it is a purely viscous phenomenon. In figure 24 the first normal stress coefficient in shear, made dimensionless with $n_p\xi^2a^4$, is plotted versus Wi or Wi^{FENE}. The curves for the FENE dumbbell and the bead–rod chain are qualitatively very similar, but the FENE dumbbell first normal stress coefficient is approximately twice the bead–rod chain value for all values of Wi. The FENE dumbbell and bead–rod chain extensional viscosity, made dimensionless with $n_p\xi a^2$, versus Wi or Wi^{FENE} is shown in figure 25. The sharp transition in the bead–rod extensional viscosity is well described by the FENE dumbbell, but the magnitude of the FENE dumbbell viscosity is up to twice that of the bead–rod chain. We note that we could have arbitrarily chosen the drag on one bead of the FENE dumbbell to be equal to the drag on half of the bead–rod chain, or equivalently $\zeta = N/2\xi$. This choice would shift the FENE dumbbell results up by a factor of 1.49 but not change the qualitative features.

From the previous comparisons we see that the FENE dumbbell and the bead–rod chain have similar rheological behaviour over a broad range of Wi in steady shear and uniaxial extensional flow, though we note that the physical basis for the stress at moderate to large Wi is different. The FENE dumbbell stress is purely Brownian and diverges as the chain becomes fully extended while the bead–rod chain has both viscous and Brownian stresses that attain limiting values as the chain becomes fully extended. In general, the FENE dumbbell model is useful for capturing the physics of the more complicated bead–rod chain in steady shear and uniaxial extensional flow for $Wi < O(100)$ where the stress is mostly Brownian.

12. Conclusions

We have presented the rheological and optical properties of a dilute suspension of bead–rod chains in two model linear flows: simple shear and uniaxial extensional flow,

https://doi.org/10.1017/S0022112096004302 Published online by Cambridge University Press

where the dimensionless flow strengths were characterized by a simulated Weissenberg number. Due to the rigid constraints, a mid-point algorithm was used which is consistent with the Stratonovich interpretation of the Brownian forces. The Giesekus form of the stress tensor was used for all steady-state simulations. We developed a modified form of the Kramers–Kirkwood stress tensor that is consistent with the Stratonovich interpretation of the Brownian forces and filters out $O(\delta t^{-1/2})$ fluctuations. In addition we developed a method to explicitly calculate the Brownian and viscous contributions to the stress tensor.

The characteristic long-time chain relaxation of initially straight chains calculated from the birefringence and stress decay both scale with N^2 and are equal to within the error of the simulations. The stress-optic coefficient at long times was shown to be constant and converged to 0.2 as N increased. The short-time birefringence decay is linear in time and exactly corresponds to the independent rotation of the $N-1$ connecting rods.

In simple shear flow the chains displayed distinct dynamics for three separate ranges of Wi. For small Wi, the viscous contribution to the shear viscosity is linear in N and an analytic expression was developed which predicted the correct scaling and magnitude of the viscosity. For moderate Wi, the polymer viscosity and first normal stress coefficient show power-law behaviour and collapse onto universal curves when plotted versus Wi. A power law for the polymer viscosity and first normal stress coefficient was derived by balancing the shear flow forces with the entropic Brownian forces. The thinning of the polymer viscosity and first normal stress coefficient at moderate Wi is found to be almost entirely due to the Brownian contributions, while the viscous contributions are relatively constant until large Wi where they showed a slight increase before thinning.

Using kinetic theory, integrals were derived for the total, viscous and Brownian viscosity of trumbells in steady extensional flow. The integrals were evaluated numerically and the results agreed very well with our Brownian dynamics simulations. For larger chains, we found that the initial increase in the extensional viscosity with increasing Wi is mostly Brownian. At large Wi the Brownian stresses plateaued to an $O(N^3)$ value which was in agreement with an analytic expression we developed for the Brownian stress in a straight bead–rod chain. Using scaling arguments we found that the Brownian and viscous contributions to the extensional viscosity were equal at a relatively large Wi ($Wi \approx 0.06N^2$) in agreement with our simulations.

For small Wi ($Wi \leqslant 3$) the stress-optic coefficient calculated using the shear viscosity, first normal stress coefficient and extensional viscosity had the relatively constant value of 0.2 in accord with the value obtained from the chain relaxation simulations. The stress-optic coefficient begins to decrease at moderate Wi due to large Brownian stresses which arise from the correlated orientations of the links. It continues to decrease at high Wi because the viscous stresses become large.

We compared simulations of a 100-bead chain to Brownian dynamics of FENE dumbbells where the FENE parameters were chosen to be consistent with the 100-bead chain. The FENE dumbbell was able to qualitatively and to some degree quantitatively predict the more complex bead–rod model for $Wi < 100$. For larger Wi additional viscous stresses must be incorporated into the FENE stress tensor to mimic a bead–rod chain.

Lastly, we are currently performing simulations of bead–rod chains in transient strong flows. We shall use these to investigate correlations in the radius-of-gyration tensor with the associated viscous and Brownian stresses for subsequent incorporation into a dumbbell model for the rheology of such solutions.

https://doi.org/10.1017/S0022112096004302 Published online by Cambridge University Press

E.S.G.S. would like to thank the National Science Foundation for supporting this work under the CPIMA Cooperative Agreement DMR-9400354-2, and the David and Lucile Packard foundation for funding through their fellowship program.

Appendix

In §10 we presented the extensional viscosity and the Brownian and viscous components for $N = 3$, a trumbell, in steady extensional flow. In this Appendix we show the integrals used to obtain our numerical results. The problem formulation follows the notation and method of Hassager (1974) and for further details the reader should refer to that work.

The dimensionless viscous tensions for a trumbell in extensional flow are

$$T^1 = \frac{\left(u_i^2 u_j^2 u_k^1 u_k^2 + 0.5 u_i^1 u_j^1\right) Pe(\delta_{i1}\delta_{j1} - 0.5\delta_{i2}\delta_{j2} - 0.5\delta_{i3}\delta_{j3})}{2 - 0.5 u_n^1 u_n^2 u_l^1 u_l^2}, \tag{A 1}$$

$$T^2 = 0.5 u_i^2 u_j^2 Pe(\delta_{i1}\delta_{j1} - 0.5\delta_{i2}\delta_{j2} - 0.5\delta_{i3}\delta_{j3}) + 0.5 T^1 u_k^1 u_k^2. \tag{A 2}$$

The viscous contribution to the polymer extensional viscosity is then

$$\eta^{p,visc} = \left(\delta_{i3}\delta_{j3} - \delta_{i1}\delta_{j1}\right)\left(R_i^1 T^1 u_j^1 + R_i^2 (T^2 u_j^2 - T^1 u_j^1) - R_i^3 T^2 u_j^2\right)/Pe, \tag{A 3}$$

and using equations (5.12) and (10.2) the polymer contribution to the extensional viscosity is

$$\eta^p = \sum_{v=1}^{3} \left(R_1^v R_1^v + 0.5 R_3^v R_3^v\right). \tag{A 4}$$

The Brownian contribution is just the difference $\eta^p - \eta^{p,visc}$.

The steady-state distribution function for the chain in extensional flow is a function of ϕ and C which are well known for a trumbell (Bird *et al.* 1978):

$$\phi = \tfrac{1}{2} Pe(\delta_{i1}\delta_{j1} - 0.5\delta_{i2}\delta_{j2} - 0.5\delta_{i3}\delta_{j3}) \sum_{v=1}^{3} R_i^v R_j^v, \tag{A 5}$$

$$C = c_1 \sin^2\chi \sin^2\beta(1 - 0.25\cos^2\chi), \tag{A 6}$$

where c_1 is a normalization constant, while χ and β are two angles associated with the trumbell's generalized coordinates (Hirschfielder, Curtiss & Bird 1964). Lastly, the bead positions must be converted into the generalized coordinates. The coordinate transformation is straightforward and can be found in Hassager (1974).

The average total polymer viscosity and viscous contribution are then given by the following integrals:

$$\langle \eta^p \rangle = \frac{\int_{\alpha=0}^{2\pi}\int_{\beta=0}^{\pi}\int_{\gamma=0}^{2\pi}\int_{\chi=0}^{\pi} \eta^p \, \mathrm{e}^{\phi} \, C^{1/2} \, \mathrm{d}\chi\mathrm{d}\gamma\mathrm{d}\beta\mathrm{d}\alpha}{\int_{\alpha=0}^{2\pi}\int_{\beta=0}^{\pi}\int_{\gamma=0}^{2\pi}\int_{\chi=0}^{\pi} \mathrm{e}^{\phi} \, C^{1/2} \, \mathrm{d}\chi\mathrm{d}\gamma\mathrm{d}\beta\mathrm{d}\alpha}, \tag{A 7}$$

$$\langle \eta^{p,visc} \rangle = \frac{\int_{\alpha=0}^{2\pi}\int_{\beta=0}^{\pi}\int_{\gamma=0}^{2\pi}\int_{\chi=0}^{\pi} \eta^{p,visc} \, \mathrm{e}^{\phi} \, C^{1/2} \, \mathrm{d}\chi\mathrm{d}\gamma\mathrm{d}\beta\mathrm{d}\alpha}{\int_{\alpha=0}^{2\pi}\int_{\beta=0}^{\pi}\int_{\gamma=0}^{2\pi}\int_{\chi=0}^{\pi} \mathrm{e}^{\phi} \, C^{1/2} \, \mathrm{d}\chi\mathrm{d}\gamma\mathrm{d}\beta\mathrm{d}\alpha}. \tag{A 8}$$

The integrals were evaluated using a standard mid-point algorithm.

https://doi.org/10.1017/S0022112096004302 Published online by Cambridge University Press

REFERENCES

Acierno, D., Titomanlio, G. & Marrucci, G. 1974 Dilute solution rheology of flexible macromolecules. *J. Polymer Sci.*, **12**, 2177–2187.

Allen, M. P. & Tildesley, D. J. 1987 *Computer Simulation of Liquids.* Clarendon Press.

Bird, R. B., Curtiss, C. F., Armstrong, R. C. & Hassager, O. 1987 *Dynamics of Polymeric Liquids: Volume 2, Kinetic Theory*. John Wiley and Sons.

Doi, M. 1990 Effects of Viscoelasticity on Polymer Diffusion. In *Dynamics and Patterns in Complex Fluids: New Aspects of Physics and Chemistry of Interfaces* (ed. A. Onuki & K. Kawasaki). Springer.

Doi, M. & Edwards, S. F. 1986 *The Theory of Polymer Dynamics.* Oxford Science Publications.

Doyle, P. S., Shaqfeh, E. S. G. & Gast, A. P. 1997 Dynamic simulation of polymers in transient linear flows. (In preparation).

Ermak, D. L. & McCammon, J. A. 1978 Brownian dynamics with hydrodynamic interactions. *J. Chem. Phys.* **69**, 1352–1360.

Fixman, M. 1978 Simulation of polymer dynamics. i. general theory. *J. Chem. Phys.* **69**, 1527–1537.

Flory, P. J. 1989 *Statistical Mechanics of Chain Molecules.* Oxford University Press.

Fuller, G. G. 1990 Optical rheometry. *Ann. Rev. Fluid Mech.* **22**, 387–417.

Gardiner, C. W. 1985 *Handbook of Stochastic Methods.* Springer.

Grassia, P. S. & Hinch, E. J. 1996 Computer simulations of polymer chain relaxation via Brownian motion. *J. Fluid Mech.* **308**, 255–288.

Grassia, P. S., Hinch, E. J. & Nitsche, L. C. 1995 Computer simulations of Brownian motion of complex systems. *J. Fluid Mech.* **282**, 373–403.

Guth, E. & Mark, H. 1934 Internal molecular statistics, especially in chain molecules. I. *Mh. Chem.* **65**, 93.

Hassager, O. 1974 Kinetic theory and rheology of bead–rod models for macromolecular solutions. i. equilibrium and steady flow. *J. Chem. Phys.* **60**, 2111–2124.

Hinch, E. J. 1976*a* The distortion of a flexible inextensible thread in a shearing flow. *J. Fluid Mech.* **74**, 317–333.

Hinch, E. J. 1976*b* The deformation of a nearly straight thread in a shearing flow with weak Brownian motions. *J. Fluid Mech.* **75**, 765–775.

Hinch, E. J. 1994*a* Brownian motion with stiff bonds and rigid constraints. *J. Fluid Mech.* **271**, 219–234.

Hinch, E. J. 1994*b* Uncoiling a polymer molecule in a strong extensional flow. *J. Non-Newtonian Fluid Mech.* **54**, 209–230.

Hinch, E. J. & Leal, L. G. 1972 The effect of Brownian motion on the rheological properties of a suspension of non-spherical particles. *J. Fluid Mech.* **52**, 683–712.

Hirschfelder, C. F., Curtiss, C. W. & Bird, R. B. 1964 *Molecular Theory of Gases and Liquids.* Wiley.

Kannan, R. M. & Kornfield, J. A 1994 Stress-optical manifestations of molecular and microstructural dynamics in complex polymer melts. *J. Rheol.* **38**, 1127–1150.

Kramers, H. A. 1946 The behaviour of macromolecules in inhomogeneous flows. *J. Chem. Phys.* **14**, 415–424.

Kröger, M., Loose, W. & Hess, S. 1993 Rheology and structural changes of polymer melts via nonequilibrium molecular dynamics. *J. Rheol.* **37**, 1057–1079.

Kuhn, W. 1934 The shape of fibrous molecules in solution. *Kolloidzschr.* **68**, 2.

Kuhn, W. & Grun, F. 1942 Relationships between elastic constants and stretching double refraction of highly elastic substances. *Kolloid Z.* **101**, 248.

Larson, R. G. 1988 *Constitutive Equations for Polymer Melts and Solutions.* Butterworths.

Larson, R. G. 1990 The unraveling of a polymer chain in a strong extensional flow. *Rheol. Acta* **29**, 371–384.

Liu, T. W. 1989 Flexible polymer chain dynamics and rheological properties in steady flows. *J. Chem. Phys.* **90**, 5826–5842.

McQuarrie, D. A. 1973 *Statistical Thermodynamics.* University Science Books.

Milner, S. T. 1991 Hydrodynamics of semidilute polymer solutions. *Phys. Rev. Lett.* **66**, 1477–1480.

Müller-Plathe, F., Rogers, S. C. & van Gunsteren, W. F. 1992 Computational evidence for

https://doi.org/10.1017/S0022112096004302 Published online by Cambridge University Press

anomalous diffusion of small molecules in amorphous polymers. *Chem. Phys. Lett*. **199**, 237–243.

Öttinger, H. C. 1994 Brownian dynamics of rigid polymer chains with hydrodynamic interactions. *Phys. Rev*. E **50**, 2696–2701.

Öttinger, H. C. 1995 *Stochastic Processes In Polymeric Fluids*. Springer.

Rallison, J. M. & Hinch, E. J. 1988 Do we understand the physics in the constitutive equation? *J. Non-Newtonian Fluid Mech*. **29**, 37–55.

Ramanathan, R., Headley, D. L. & Lai, S. Y. 1995 Extensional viscosity of polyolefins via flow visualization. *ANTEC Conf. Proc*. **1**, 1073-1077.

Russel, W. B., Saville, D. A. & Schowalter, W. R. 1989 *Colloidal Dispersions*. Cambridge University Press.

Ryckaert, J. P., Ciccotti, G., & Berendsen, J. 1977 Numerical integration of the Cartesian equations of motion of a system with constraints: molecular dynamics of n-alkanes. *J. Comput. Phys*. **23**, 327–341.

Stewart, W. E. & Sorensen, J. P. 1972 Hydrodynamic interaction effects in rigid dumbbell suspensions. ii computations for steady shear flow. *Trans. Soc. Rheol*. **16**, 1–13.

Talwar, K. K. & Khomami, B. 1995 Flow of viscoelastic fluids past periodic square arrays of cylinders: inertial and shear thinning viscosity and elasticity effects. *J. Non-Newtonian Fluid Mech*. **57**, 177–202.

Treloar, L. R. G. 1975 *The Physics of Rubber Elasticity*, 3rd Edn. Clarendon Press.

Wales, J. L. S. 1976 *The Application of Flow Birefringence to Rheological Studies of Polymer Melts*. Delft University Press.

Warner, H. R. 1972 Kinetic theory and rheology of dilute suspensions of finitely extendible dumbbells. *Ind. Eng. Chem. Fundam*. **11**, 379–387.

Wedgewood, L. E. & Ostrov, D. N. & Bird, R. B. 1991 A finitely extensible bead-spring chain model for dilute polymer solutions. *J. Non-Newtonian Fluid Mech*. **40**, 119–139.

Xu, Z., Kim, S. & Pablo, J. J. de 1994 Anisotropic friction and excluded volume effects in freely jointed bead–rod polymer chain models. *J. Chem. Phys*. **101**, 5293–5304.

https://doi.org/10.1017/S0022112096004302 Published online by Cambridge University Press